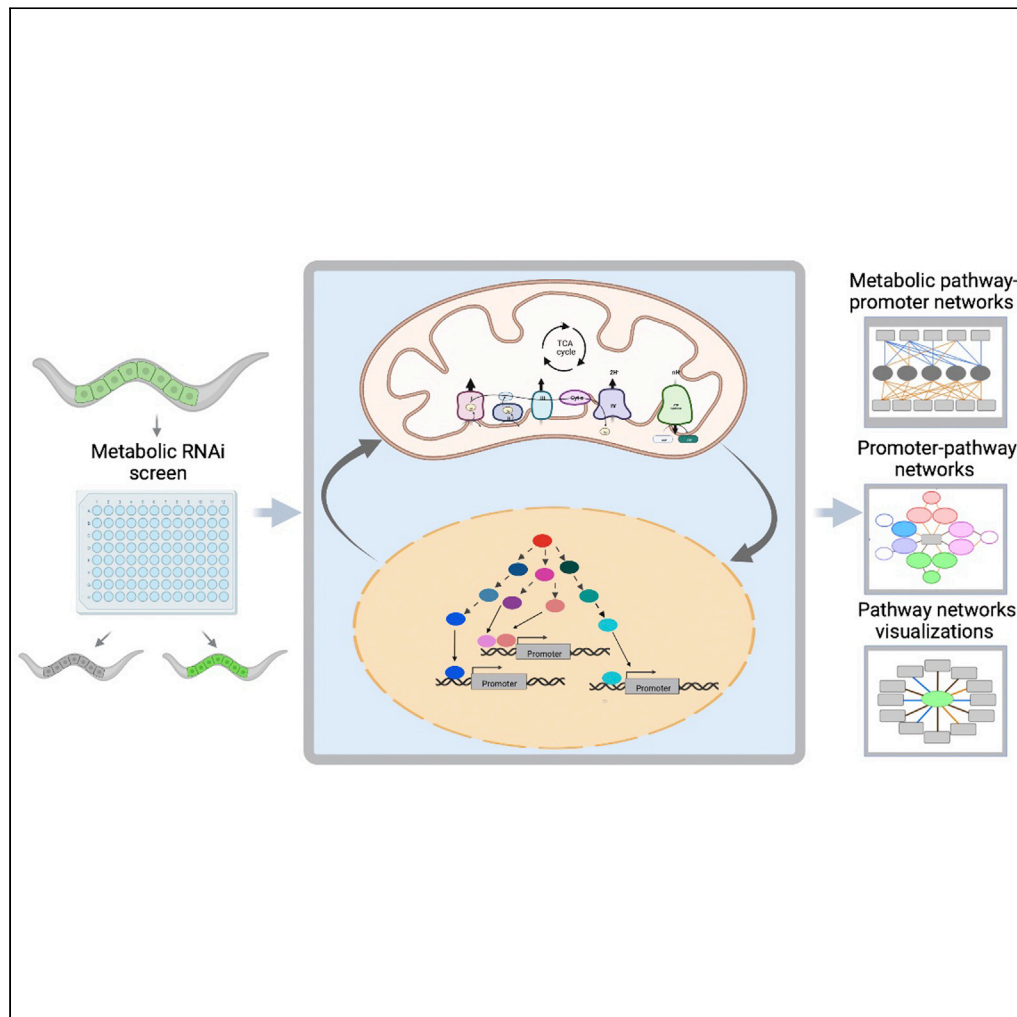


Article

A metabolic regulatory network for the *Caenorhabditis elegans* intestine

Sushila
Bhattacharya,
Brent B. Horowitz,
Jingyan Zhang, ...,
Gabrielle E. Giese,
Amy D. Holdorf,
Albertha J.M.
Walhout

marian.walhout@umassmed.
edu

Highlights

RNAi screen delineates
the first animal intestinal
metabolic regulatory
network

In contrast to TF
knockdown, metabolic
gene RNAi mainly
activates promoter
activity

Lipid, amino acid, and
energy metabolism
changes impact promoter
activity the most

Several TFs that modulate
promoter expression
downstream of the ETC
were identified

Bhattacharya et al., iScience
25, 104688
August 19, 2022 © 2022 The
Author(s).
[https://doi.org/10.1016/
j.isci.2022.104688](https://doi.org/10.1016/j.isci.2022.104688)

Article

A metabolic regulatory network for the *Caenorhabditis elegans* intestineSushila Bhattacharya,¹ Brent B. Horowitz,¹ Jingyan Zhang,^{1,2} Xuhang Li,¹ Hefei Zhang,¹ Gabrielle E. Giese,¹ Amy D. Holdorf,¹ and Albertha J.M. Walhout^{1,3,*}

SUMMARY

Metabolic perturbations can affect gene expression, for instance to rewire metabolism. While numerous efforts have measured gene expression in response to individual metabolic perturbations, methods that determine all metabolic perturbations that affect the expression for a given gene or set of genes have not been available. Here, we use a gene-centered approach to derive a first-pass metabolic regulatory network for *Caenorhabditis elegans* by performing RNAi of more than 1,400 metabolic genes with a set of 19 promoter reporter strains that express a fluorescent protein in the animal's intestine. We find that metabolic perturbations generally increase promoter activity, which contrasts with transcription factor (TF) RNAi, which tends to repress promoter activity. We identify several TFs that modulate promoter activity in response to perturbations of the electron transport chain and explore complex genetic interactions among metabolic pathways. This work provides a blueprint for a systems-level understanding of how metabolism affects gene expression.

INTRODUCTION

Metabolism, broadly defined as the combination of reactions that digest nutrients and produce biomass and energy, is central to most if not all biological processes. Therefore, metabolic perturbations, whether genetic, environmental, or nutritional, can affect these processes not only at the level of overall physiology but also molecularly, for instance by modulating gene expression. Numerous studies in model organisms and humans have identified gene expression changes in response to metabolic perturbations and studied the transcriptional mechanisms involved. Classical examples in microbes include the changes in gene expression upon a shift in carbon source, which serves to rewire metabolism as needed. For instance, when shifted from glucose to lactose, the *Escherichia coli* transcription factor (TF) *Lacl* is removed from the *Lac* operon, allowing *Lac* gene expression (Gilbert and Muller-Hill, 1966; Jacob and Monod, 1961). Similarly, the yeast *Saccharomyces cerevisiae* uses the TF Gal4p to activate a specific gene expression program when galactose is introduced as a carbon source (Johnston, 1987). Metabolic perturbations also affect gene expression in metazoan organisms and humans. One of the best-known examples is the activation of cholesterol biosynthesis genes by the TF SREBP, which translocates to the nucleus when cholesterol levels are low (Wang et al., 1994; Yokoyama et al., 1993).

With the advent of expression profiling techniques such as RNA sequencing (RNA-seq), it has become feasible to rapidly and comprehensively identify gene expression changes in response to different nutritional, environmental, or genetic conditions. As a result, an enormous amount of gene expression profiling data is available for many model organisms and humans. Moreover, gene expression profiles can be measured with increasing depth at the level of single cells. Therefore, it has become feasible to measure gene expression changes in response to specific metabolic and genetic perturbations. For instance, an early landmark study in yeast used a highly integrated experimental and modeling approach to study perturbations in the GAL pathway (Ideker et al., 2001). However, complementary methods with which one can comprehensively identify the perturbations that affect a gene, or set of genes, of interest, have not yet been available. Here, we use such a “gene-centered” approach to comprehensively study the metabolic perturbations that affect the activity of each of 19 promoters in the nematode *Caenorhabditis elegans*.

C. elegans is a powerful model system to study numerous biological processes, including development, behavior, and aging (Nigon and Felix, 2017). Many RNA-seq datasets are available for *C. elegans*, and

¹Department of Systems Biology, University of Massachusetts Chan Medical School, Worcester, MA 01605, USA

²Present address: Shanghai Key Laboratory of Metabolic Remodeling and Health, Institute of Metabolism and Integrative Biology, Fudan University, Shanghai 200433, China

³Lead contact

*Correspondence: marian.walhout@umassmed.edu

<https://doi.org/10.1016/j.isci.2022.104688>



the animal has been used in pioneering single-cell expression profiling studies (Cao et al., 2017; Packer et al., 2019). More recently, *C. elegans* has been established as a premier model to study metabolism (Watson and Walhout, 2014; Watts and Ristow, 2017). The *C. elegans* intestine is a highly metabolic tissue that breaks down ingested nutrients and delivers these to other tissues (McGhee, 2007). A genome-scale metabolic network model has been constructed and multiple metabolic pathways have been carefully annotated and visualized (Walker et al., 2021; Yilmaz et al., 2020; Yilmaz and Walhout, 2016). There are several examples of gene expression changes that occur in response to metabolic perturbations in *C. elegans*. One example in the intestine is the transcriptional activation of a propionate shunt when the canonical, vitamin B₁₂-dependent breakdown pathway of this short chain fatty acid is nutritionally or genetically perturbed (Watson et al., 2014, 2016). The first gene of the propionate shunt, the acyl-CoA dehydrogenase *acdh-1*, is activated by low vitamin B₁₂ diets via two transcriptional mechanisms. Low B₁₂ mechanism-I involves the nuclear hormone receptors (NHRs) *nhr-10* and *nhr-68* that together act as a transcriptional persistence detector in response to the sustained accumulation of propionate (Bulcha et al., 2019). Low B₁₂ mechanism-II is activated in response to low activity of the vitamin B₁₂-dependent methionine/S-adenosylmethionine (Met/SAM) cycle and involves another NHR, *nhr-114*, which responds to low SAM levels (Giese et al., 2020). However, for other metabolic perturbations that activate *acdh-1*, the underlying transcriptional mechanisms remain unknown (Watson et al., 2013).

We previously developed a gene-centered method to delineate a gene regulatory network (GRN) in which we used a set of 19 promoter reporters that express a fluorescent protein in the *C. elegans* intestine (MacNeil et al., 2015). By performing systematic RNAi of almost all ~1,000 TFs (Reece-Hoyes et al., 2005), we identified those that, when knocked down, resulted in a visible change in fluorescent protein levels in this tissue. Surprisingly, by analyzing this GRN, we found that many TFs affect promoter activity indirectly, i.e., because they were not found to physically interact with the promoter either by ChIP or by yeast one-hybrid assays (Fuxman Bass et al., 2016; Gerstein et al., 2010; MacNeil et al., 2015; Van Nostrand and Kim, 2013).

Here, we delineated the first intestinal “metabolic regulatory network” (MRN) for an animal. Specifically, we performed systematic RNAi of more than 1,400 metabolic genes to identify those whose function affects the activity of the same 19 reporters we used previously. We found that metabolic perturbations affect each promoter, albeit to a different extent and that changes in promoter activity occur with perturbations in lipid, amino acid, and energy metabolism, but much less with perturbations in carbohydrate metabolism. Remarkably, metabolic perturbations predominantly increase promoter activity, which is in contrast to RNAi of TFs, which tends to repress promoter activity (MacNeil et al., 2015). We identified several TFs that mediate the response to perturbations in the electron transport chain (ETC), including the activation of *acdh-1* by ETC complex II inhibition, and the activation of *nhr-178* by ETC complex III inhibition. Finally, we explored complex interactions among metabolic pathways in regulating *acdh-1* promoter activity. Our study provides a blueprint for understanding the intricate relationships between metabolism and gene expression at a network, or systems, level.

RESULTS

A *C. elegans* intestinal metabolic regulatory network

To examine how perturbations in *C. elegans* metabolism affect promoter activity, we first constructed an updated RNAi library of metabolic genes. We previously generated an RNAi library of 836 metabolic genes that were curated based on Kyoto Encyclopedia of Genes and Genomes (KEGG) and WormBase descriptions (Watson et al., 2016). We removed genes that were not directly relevant to metabolic reactions (e.g., DNA and RNA polymerases), added known metabolic genes absent from the original library, and removed duplicates, transposons, and pseudogenes for a total of 1,495 unique metabolic genes referred to as met-2.0 (Table S1).

We performed RNAi with this metabolic gene library and the same 19 intestinal reporter strains we previously used to identify regulating TFs (MacNeil et al., 2015) (Table S2; Figure 1A). These promoters drive the expression of a protein or a microRNA in the animal’s intestine and other tissues. Protein-coding gene promoters include those corresponding to metabolic genes (*acdh-1*, *acdh-2*, *acs-19*, and *gpd-3*), stress-related genes (*gst-4*, *bli-3*, *sod-3*, *hsp-3*, *hsp-4*, and *irg-5*), and TFs (*sbp-1*, *nhr-178*, and *mdl-1*). MicroRNA promoters include *mir-63*, *let-7*, and *mir-71*. Each reporter was visually screened in triplicate for changes in fluorescent protein levels in the intestine, which amounts to more than 85,000 visual assessments. Screens

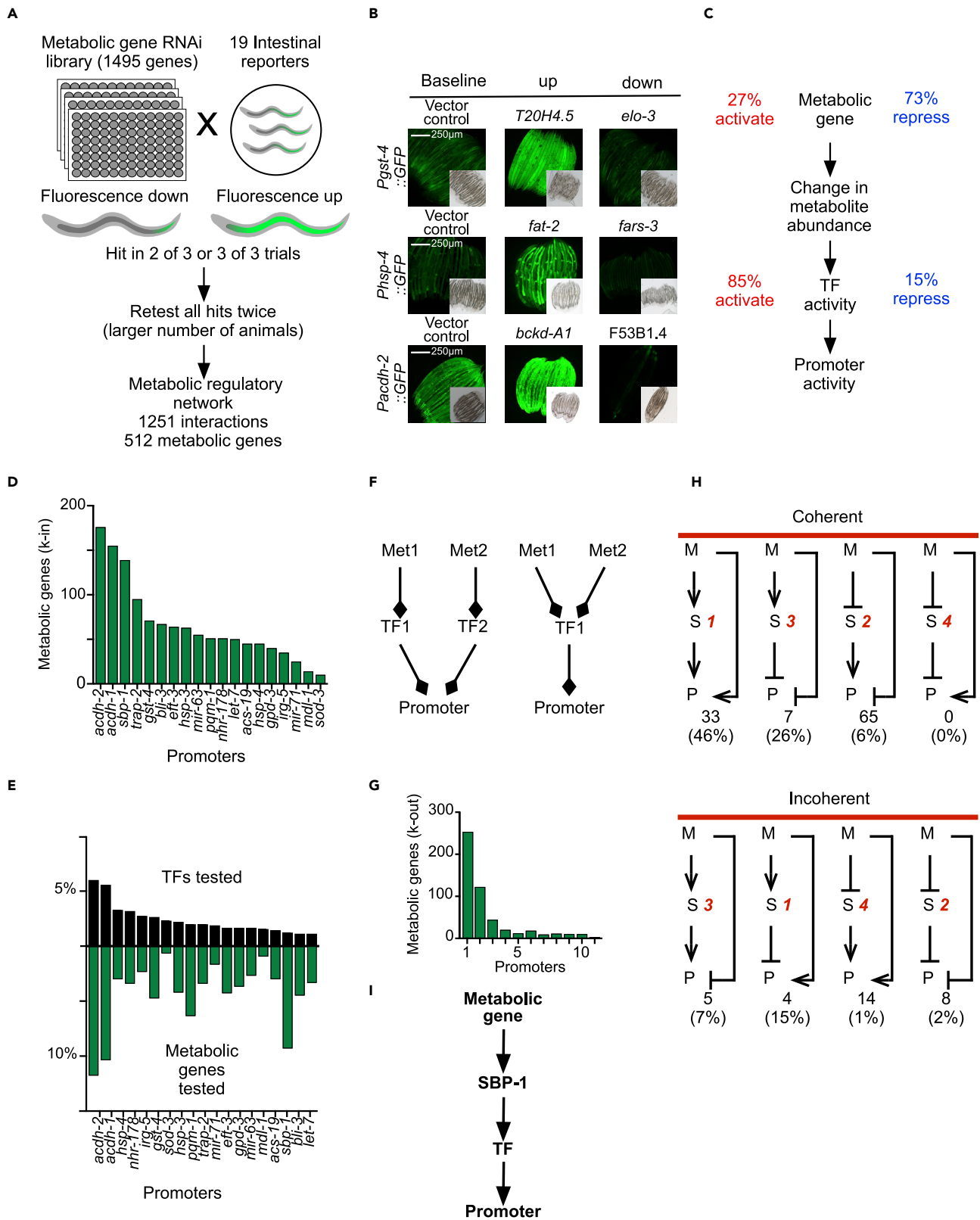


Figure 1. A *C. elegans* intestinal metabolic regulatory network

- (A) Outline of RNAi screen with 19 intestinal reporter strains using the met-2.0 library containing 1,495 metabolic genes. The primary screen was performed in triplicate, and hits were retested with all strains in duplicate. Related to [Tables S1](#) and [S2](#).
- (B) Examples of interactions between metabolic genes and intestinal gene promoters. Throughout the paper fluorescence images are shown with bright field images as insets. We used scale bar = 250µm, throughout the study.
- (C) Graph outlining potential information flow in combined MRN and GRN.
- (D) *k* refers to degree, or number of interactions. The in-degree (*k*-in) distribution of the MRN, which is defined as the number of metabolic gene knockdowns that increase or decrease promoter activity in the intestine. Related to [Table S3](#).
- (E) The percentage of TFs (top, black) versus metabolic genes (bottom, green) that regulate each intestinal promoter. Data are shown as the percent of RNAi knockdowns causing a change in promoter activity relative to the number of RNAi clones in the TF (top) or metabolic gene (bottom) RNAi library.
- (F) Two types of wiring in the combined MRN and GRN.
- (G) The out-degree (*k*-out) distribution of the MRN, which is defined as the number of intestinal gene promoters affected by each metabolic gene knockdown. Related to [Table S3](#).
- (H) Detection of each of eight possible feedforward loops involving metabolic genes (M), the TF SBP-1 (S), and downstream promoters (P). The numbers in red are according to numbering by Alon and colleagues ([Mangan and Alon, 2003](#)). Numbers and percentages below each circuit indicate total numbers and percentage of possible circuits, *i.e.*, which of the $M \rightarrow S \rightarrow P$ are confirmed by detection of $M \rightarrow P$ in the MRN, between brackets.
- (I) Diagram of potential information flow of interactions involving the TF SBP-1.

were carried out manually because 18 of the 19 reporters also drive expression in at least one other tissue ([MacNeil et al., 2015](#)). We focused on the fourth larval (L4) stage, as described previously ([MacNeil et al., 2015](#)). All hits found in two or three of the replicates were retested twice with all 19 intestinal reporters, using larger plates and more animals. Interactions received a confidence score based on how frequently the effect was observed relative to the number of tests and only interactions observed at least twice were kept in the final network ([Table S3](#)). Examples of metabolic genes that regulate intestinal promoter activity are shown in [Figure 1B](#).

The intestinal MRN contains 1,251 regulatory interactions between 19 promoters and 512 metabolic genes ([Table S3](#)). Interestingly, most of the interactions involving metabolic genes were repressing (increased fluorescence after RNAi). This is in contrast to the intestinal GRN, where we found that most TF knockdowns resulted in a decrease in fluorescence ([Figure 1C](#)) ([MacNeil et al., 2015](#)). This observation suggests that metabolic perturbations tend to activate gene expression through TFs that activate expression of their target genes.

Large-scale visual screens like the one presented here are error prone, especially when many conditions are screened versus many genes in triplicate, in part because the human eye gets tired and due to variability in RNAi knockdown. Additionally, some reporters (*Pirg-5::GFP* and *Phsp-4::GFP*) have fainter GFP expression making it easier to score for increased GFP upon RNAi as compared to decreased GFP. Conversely, *Pacdh-2::GFP* expresses GFP strongly in other tissues, making it more difficult to screen for increased GFP in the intestine. Furthermore, reporters that are tagged with mCherry (*Phsp-3::GFP*, *Peft-3::GFP*, and *Ptrap-2::GFP*) and are nuclear localized, are harder to screen because mCherry is relatively faint. This variation in brightness of the reporters could contribute to false negatives (missed interactions). Additionally, some reporter transgenes are not integrated into the genome, *i.e.*, are present as a multi-copy array (*Pbli-3::GFP* and *Pspb-1::GFP*), which results in mosaicism that may be interpreted as a change in fluorescence due to the RNAi. To estimate the noise in the primary screen, we compared the regulatory interactions found for the *acdh-1* promoter in our primary screen to our previous data from a whole genome RNAi screen for *Pacdh-1::GFP* ([Watson et al., 2013](#)). In our previous study, we used the ORFeome RNAi library ([Rual et al., 2004](#)) and screened for genes that increased and decreased fluorescence in *Pacdh-1::GFP* animals. Of the 50 genes that were previously found to regulate *Pacdh-1::GFP* and that were also included in the updated metabolic RNAi library, 25 were detected ([Table S4](#)) ([Watson et al., 2013](#)). This illustrates the noise in large-scale, visual RNAi screens (see Discussion).

The number of metabolic genes affecting a promoter (the in-degree, or *k*-in) ranged from 10 to 176, with an average and median number of 66 and 51 metabolic genes, respectively ([Figure 1D](#)). Seven of the intestinal promoters drive the expression of a metabolic enzyme (*acdh-1*, *acdh-2*, *gst-4*, *bli-3*, *acs-19*, *gpd-3*, and *sod-3*) ([Walker et al., 2021](#)) and changes in their activity in response to metabolic gene knockdown may indicate transcriptional rewiring of metabolism. Next, we asked whether promoter connectivity (*i.e.*, *k*-in) in the MRN correlates with connectivity in the GRN. Overall, we did not observe a clear correlation, with the exception of the promoters of *acdh-1* and *acdh-2*, which are highly connected in both networks ([Figure 1E](#) and [Table S3](#)). Overall, these observations suggest that there are distinct types of interactions involved in

the metabolic control of gene expression. Promoters that are affected by many metabolic perturbations and many TFs may use distinct TFs to respond to different types of metabolic perturbations, while promoters that are highly connected only in the MRN may respond to metabolic perturbations via the same, or a limited set of TF(s) (Figure 1F).

Finally, we examined the connectivity of different metabolic genes in the MRN (the out-degree, or k-out) and found that 73% of metabolic genes in the MRN tested affect only one or two promoters when knocked down (Figure 1G). This is highly similar to the out-degree of the GRN we previously delineated, where 77% of TFs in the GRN regulated only one or two promoters (MacNeil et al., 2015). Together, these data show that the GRN and MRN exhibit a similar organization, with one major difference: TF knockdown tends to repress promoter activity, while RNAi of metabolic genes activates the same set of promoters.

SBP-1 is a TF and the *sbp-1* promoter is also part of the set of 19 reporter strains (MacNeil et al., 2015). In the GRN, we found that SBP-1 regulates 12 of the 19 promoters, including its own. This observation allowed us to ask a simple question: how often does RNAi of a metabolic gene that activates or represses the *sbp-1* promoter affect other promoters that are affected by the SBP TF? To answer this question, we used the concept of feedforward loops (FFLs), which capture this type of sequential regulation and allows us to assess our dataset. Briefly, in FFLs, a regulator affects another regulator, and both affect the same downstream gene. In coherent FFLs, each arm has the same regulatory effect; i.e. both arms either repress or activate the downstream gene. In incoherent FFLs, the arms have opposite effects on the downstream gene, i.e., one arm represses and the other activates (Bulcha et al., 2019; Mangan and Alon, 2003). Here, we specifically examine metabolic genes that affect both the *sbp-1* promoter and each of the 18 other promoters and ask for each combination whether SBP-1 was found to regulate the same promoter in our previous dataset (MacNeil et al., 2015). There are eight possible FFLs, where the different interactions are activating or repressing. For each of these, we determined the possible configurations that could have been detected and then calculated the proportion actually detected in the combined MRN/GRN dataset (Figure 1H). Overall, we found that of all possible type 1 FFLs, 46% were detected in the dataset, while the proportion of other types of FFLs was detected with much lower frequency. This observation indicates that metabolic perturbations that repress *sbp-1* expression most frequently translate to a repression of downstream promoter activity. An example includes RNAi of *fasn-1*, which represses the *acs-19* and *sbp-1* promoter (Table S3), and RNAi of *sbp-1*, which represses the *acs-19* promoter (MacNeil et al., 2015). It is important to note that such FFLs are not direct, but rather indicate structure in the GRN/MRN datasets. Specifically, the concept of FFLs was used here to investigate concordance between the TF RNAi and metabolic gene RNAi datasets. In reality, these FFLs may function as indicated, may function as simple linear cascades, or may be more indirect by involving additional regulators.

In the simplest FFLs, SBP-1 directly binds a promoter and regulates its activity. However, we could not examine this because there are no available datasets for physical protein-DNA interactions involving SBP-1, either by chromatin immunoprecipitation (Gerstein et al., 2010) or by yeast one-hybrid assays (Fuxman Bass et al., 2016). This is likely because SBP-1 is localized to membranes and needs to be cleaved and translocated to the nucleus upon receiving a (metabolic) stimulus, and therefore is likely not detected in yeast one-hybrid assays (Wang et al., 1994). Furthermore, our previous study indicated that SBP-1 functions high in the regulatory hierarchy and may affect promoter activity indirectly, for instance by repressing or activating the expression of other TFs (MacNeil et al., 2015). Given that SBP-1 acts high in the regulatory hierarchy (MacNeil et al., 2015), this suggests that repression of *sbp-1* expression results in downregulation of a TF that activates promoter activity (Figure 1I).

Pathway-level MRN integration

Metabolism is organized into different pathways and complexes that together form the metabolic network. Previously, we constructed a *C. elegans* genome-scale metabolic network based on enzyme homology and annotations available in various databases such as KEGG and BRENDA (Yilmaz and Walhout, 2016). We recently updated this model to the current version, iCEL1314, which includes additional gene and reaction annotations (Yilmaz et al., 2020), and carefully annotated 85 *C. elegans* metabolic pathways and categories to generate 62 pathway maps that can be found on the WormFlux website (<http://wormflux.umassmed.edu/>) (Walker et al., 2021; Yilmaz and Walhout, 2016). Pathways indicate connected metabolic reactions (e.g., leucine degradation) and categories include complexes and groups of functionally related proteins (e.g., ETC complex I). For simplicity, we refer to both pathways and categories as pathways. Pathways were

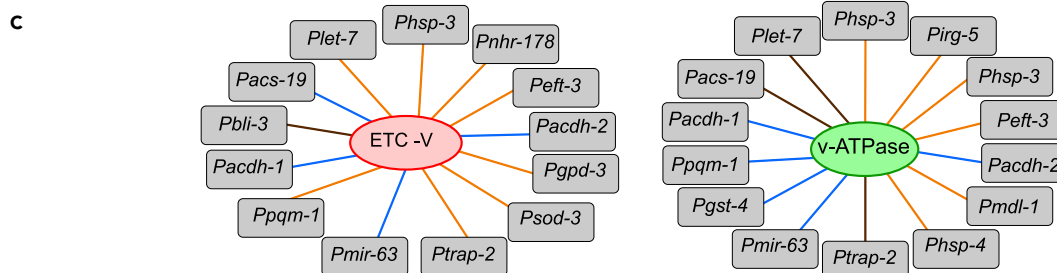
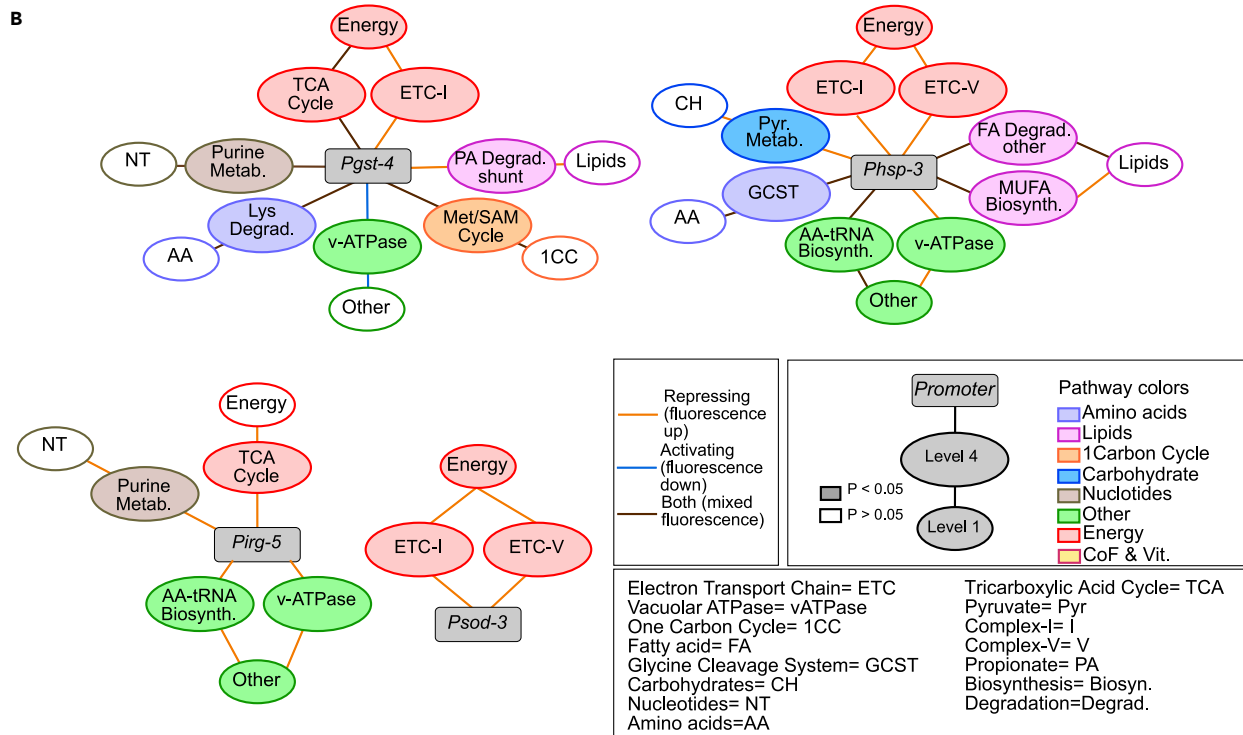
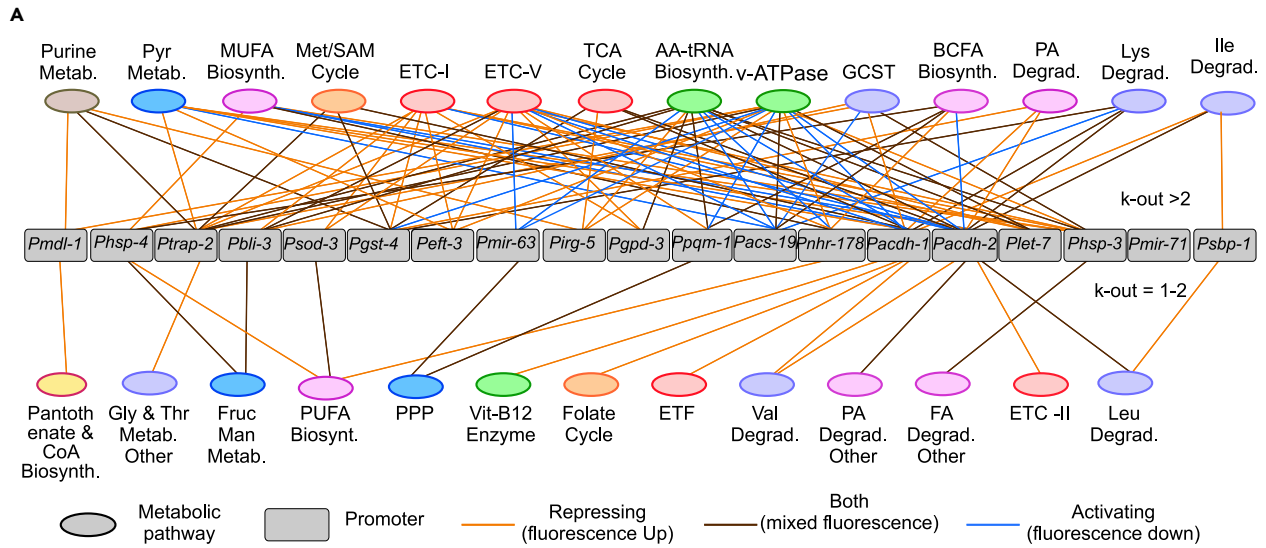


Figure 2. Metabolic pathway enrichment

(A) MRN of enriched metabolic pathways ($p < 0.05$ by hypergeometric distribution) and the 19 intestinal promoters. Promoters are represented as gray rectangles, and enriched pathways as color-coded ovals. Orange edges indicate repressing interactions (fluorescence up), blue edges indicate activating interactions (fluorescence down), and black edges indicate mixed fluorescence. K-out indicates the number of promoters regulated by each pathway. Related to [Table S5](#).

(B) Examples of four promoter-pathway networks. The connected rings start at level 1 (smaller ring) and go inward to level 4 (larger ring, closest to the promoter). Within the levels, the same pathways use the same color code. Enriched pathways ($p < 0.05$ by hypergeometric distribution) are indicated by filled ovals and non-enriched pathways ($p > 0.05$) are indicated by empty ovals. Related to [Figure S1](#) for additional promoter networks.

(C) Examples of two pathway-promoter networks. Pathways are colored as in (B). Related to [Figure S2](#) for additional enriched pathway networks.

annotated at increasing levels of resolution ([Walker et al., 2021](#)). Briefly, level 1 metabolic gene annotations are broad and are refined and narrowed to specific metabolic pathways all the way to level 4. For example, genes involved in the glycine cleavage system are first defined in the level 1 category of amino acids, then level 2 glycine, serine, and threonine metabolism, level 3 glycine and threonine metabolism, and level 4 glycine cleavage system. Since not all levels can be subdivided, redundancies exist at levels 3 and 4.

We previously found that perturbation of genes in the canonical, vitamin B12-dependent propionate breakdown pathway activates a propionate shunt, the first gene of which is *acdh-1*, whose promoter is included in this study ([Watson et al., 2013, 2016](#)). Here, we extend this concept by asking whether there was enrichment for particular metabolic pathways regulating each of the 19 promoters in the MRN. For pathway enrichment analysis, we used the pathway assignments from the iCEL1314 network model ([Walker et al., 2021](#)). At level 4, we found that 27 of the 85 metabolic pathways are enriched in the network ([Figure 2A](#); [Table S5](#)). Thus, a large fraction of metabolic pathways regulates gene expression when perturbed.

For each promoter, we visualized enriched pathways as sequentially connected circles starting with level 1 moving down to level 4 ([Figure 2B](#)). Four examples of promoter networks are shown in [Figure 2B](#): *Pgst-4* and *Phsp-3* are intermediately connected promoter networks that are enriched for seven and eight level 4 pathways, respectively; *Psod-3* and *Pirg-5* are lowly connected promoter networks with two and four level 4 pathways enriched, respectively. Promoter-pathway networks not featured in the main figures are provided in [Figure S1](#).

All 19 promoters are linked by shared pathways, showing the high degree of connectivity in the intestinal MRN. Most pathways are enriched for only one or two promoters, while others are enriched for many promoters ([Table S5](#)). Among the most highly connected pathways are vacuolar-ATPase (v-ATPase) and ETC complex V ([Figure 2C](#)). In addition, aminoacyl-tRNA-synthetase RNAi affects many promoters, and most reporters are downregulated ([Figure S2](#); [Table S3](#)). Aminoacyl-tRNA-synthetases link amino acids to their cognate tRNAs and are, therefore, critical for mRNA translation ([Rubio Gomez and Ibba, 2020](#)). Thus, the observation that most reporters used in our screen are repressed by knockdown of aminoacyl-tRNA synthetases is not surprising since the readout is based on fluorescent protein expression in the intestine. The *irg-5* promoter, however, is activated when aminoacyl-tRNA synthetases are knocked down, which agrees with previous observations ([Melo and Ruvkun, 2012](#)) ([Table S3](#)). It is interesting to note that, even though carbohydrate metabolism is a fundamental biochemical process for energy generation, knockdown of genes annotated to carbohydrate metabolism did not have a strong impact on promoter activity. Pathway networks visualizations for level 4 enriched pathways not shown in the main figures are provided in [Figure S2](#).

Broad effects of ETC perturbation on promoter activity

Many of the intestinal promoters respond to perturbation of members of the ETC, which carries out oxidative phosphorylation in the mitochondria ([Table S3](#)). When we obtained this result, we realized that only members of ETC complexes I, II, and V (ATP-synthase) were included in our primary metabolic gene RNAi library. To test the effects of ETC perturbation more comprehensively, we carefully annotated the five ETC complexes, generated a mini-library of all available RNAi clones, and used it to screen all 19 intestinal promoter strains ([Table S6](#)). We included only ETC complex components that are encoded by the nuclear genome, *i.e.*, the 12 members encoded by the mitochondrial genome were not tested. Example images of both repressing and activating interactions are shown in [Figure 3A](#). Of interactions tested in both the primary and the mini-library screen, 100 interactions were detected by both, 64

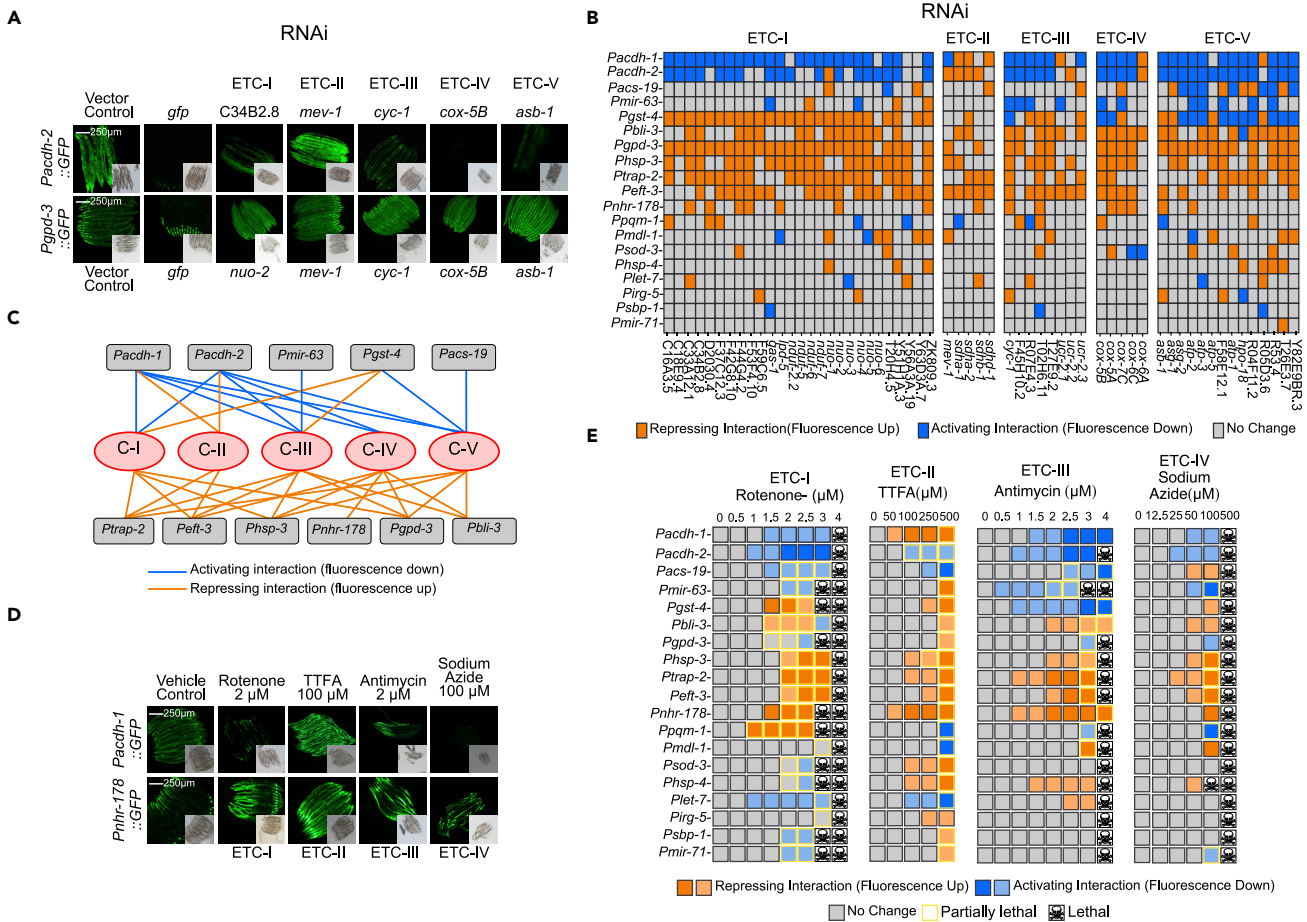


Figure 3. Electron transport chain perturbation differentially affects intestinal promoter activity

(A) Examples of *C. elegans* promoter reporter strains subjected to RNAi from different ETC complex members. (B) Overview of all ETC complex RNAi on the intestinal activity of the 19 target promoters. Related to Table S6. (C) Diagram of the ETC complex-promoter regulatory network. (D) Examples of *C. elegans* promoter reporter strains treated with ETC complex inhibitor drugs. (E) Overview of the effect of ETC complex drug treatment on the intestinal activity of the 19 target promoters.

were only found in the primary screen, and 226 only with the mini-library (Table S7). This modest overlap further illustrates the challenge of large-scale visual experiments and the need for replicate experiments. However, even with relatively noisy data, a clear picture emerged. Promoters exhibited different degrees of responses to ETC perturbation; more than half of the 19 promoters showed consistent changes in activity and most of these were activated, while some, most notably *Pacdh-1* and *Pacdh-2*, were mostly repressed (Figures 3B and 3C). Remarkably, these two promoters were activated by RNAi of ETC-complex II members, which has a dual function in both the ETC and the TCA cycle (Figure 3B, see below). Further, the *gst-4* promoter was activated by knockdown of ETC complexes I and III but repressed by ETC complex V (ATP synthase) RNAi (Figure 3B). These observations indicate that different ETC complexes can have distinct effects on promoter activity, showing that these promoters do not simply respond to changes in energy metabolism.

To validate the effects of ETC inhibition by RNAi on promoter activity, we treated animals with drugs that specifically affect different ETC complexes to each of the 19 intestinal reporter strains, including rotenone (complex I) (Palmer et al., 1968), 2-thenoyltrifluoroacetone (TTFa) (complex II) (Armson et al., 1995), antimycin A (complex III) (Slater, 1973), and sodium azide (complex IV) (Stannard and Horecker, 1947). With these drugs, we observed robust modulation of promoter activity, which, with one notable exception discussed below, largely agreed with the RNAi data (Figures 3D and 3E). We also tested oligomycin A (complex V)

(Hong and Pedersen, 2008) but did not see any changes in fluorescence at any dose in any of the strains tested.

Complex metabolic regulation of the *acdh-1* and *acdh-2* promoters

Two of the 19 intestinal promoters used in this study control the expression of two highly homologous acyl-CoA dehydrogenases, *acdh-1* and *acdh-2*. Because genes are associated with metabolic reactions based on homology with enzymes known to catalyze particular reactions, *acdh-1* and *acdh-2* are annotated to an overlapping set of metabolic reactions involved in amino acid and fatty acid degradation in the genome-scale metabolic network model (Yilmaz et al., 2020; Yilmaz and Walhout, 2016). However, we have previously shown that ACDH-1 catalyzes the first reaction in the propionate shunt, which is activated when flux through the canonical, vitamin B12-dependent propionate breakdown pathway is impaired (Watson et al., 2014, 2016). We did not find any supporting evidence that *acdh-2* also functions in this pathway (data not shown), and therefore, the biochemical function of this acyl-CoA dehydrogenase remains unknown.

In the MRN, the *acdh-1* and *acdh-2* promoters are each enriched for several metabolic pathways, including propionate degradation, the glycine cleavage system, and the methionine/S-adenosylmethionine (Met/SAM) cycle, which we have found previously to affect *acdh-1* expression (Giese et al., 2020; Watson et al., 2013) (Figure 4A). Additional enriched pathways include pyruvate metabolism, the ETC, and the tricarboxylic acid (TCA) cycle (Figure 4A). The *acdh-1* and *acdh-2* promoters are in fact the most highly connected in both the MRN and GRN, and most metabolic genes and TFs that regulate *acdh-1* also regulate *acdh-2* (Figure 4B). These include another acyl-CoA dehydrogenase, *acdh-3*, RNAi of which activates both promoters (Table S3). Remarkably, however, a small fraction of metabolic genes and TFs have opposite effects on these two promoters when knocked down: RNAi of five metabolic genes activates *acdh-1* but represses *acdh-2* promoter activity and perturbation of three TFs represses *acdh-1* but activates *acdh-2* (Figure 4C). Interestingly, while the proteins encoded by *acdh-1* and *acdh-2* share a high degree of homology (Figure S3), their promoters do not share obvious similarities and the two genes are located on different chromosomes. The observation that the *acdh-1* and *acdh-2* promoters respond to many of the same metabolic perturbations and many of the same TFs suggests that much of the regulatory wiring and non-coding elements such as TF-binding sites are shared between the two promoters.

The ETC complex II inhibitors TTFA and 3-nitropropionate have distinct effects on *acdh-2* expression and block RNAi

Since perturbation of the ETC had widespread effects on promoter activity, we wondered which TFs mediate these effects. We reasoned we could answer this question by performing RNAi against an ETC component that activates intestinal promoter activity, and then screening the TF RNAi library (MacNeil et al., 2015) to identify TFs required for this activation. However, performing RNAi with multiple genes in the same sample in *C. elegans* is unreliable (Kamath et al., 2001). Therefore, we reasoned that ETC-inhibiting drugs would present an opportunity to identify TFs that mediate promoter activation by combining such drugs with TF RNAi. To test this, we first focused on promoter activation by knockdown of ETC complex II. However, we noticed that there was one clear disagreement between the ETC RNAi data and the ETC inhibitory drugs discussed above: the *acdh-2* promoter was robustly activated by ETC complex II RNAi but repressed by the supplementation of TTFA (Figures 3B and 3E). In contrast, the promoter of its paralog *acdh-1* was induced both by ETC complex II RNAi and by TTFA supplementation (Figures 3B and 3E). Surprisingly, we found that addition of TTFA completely blocked RNAi (Figure S4C). We tested another ETC complex II inhibitory drug, 3-nitropropionate (3-NP) (Alston et al., 1977), and found that its supplementation robustly activated the *acdh-2* promoter (Figure 4D). This result shows that distinct ETC complex II inhibitory drugs have different effects on gene expression. However, like TTFA, addition of 3-NP also blocked RNAi and this effect likely occurs by interfering with bacterial growth (Figure S4B). Therefore, these drugs could not be used together with TF RNAi to investigate the transcriptional mechanisms that respond to ETC complex II perturbations.

ETC complex II inhibition activates the *acdh-1* promoter via multiple TFs and is inhibited by TCA cycle and pentose phosphate pathway perturbations

ETC complex II, or succinate dehydrogenase (SDH), participates both in oxidative phosphorylation and in the TCA cycle. It catalyzes a single reaction, the dehydrogenation of succinate to fumarate and the

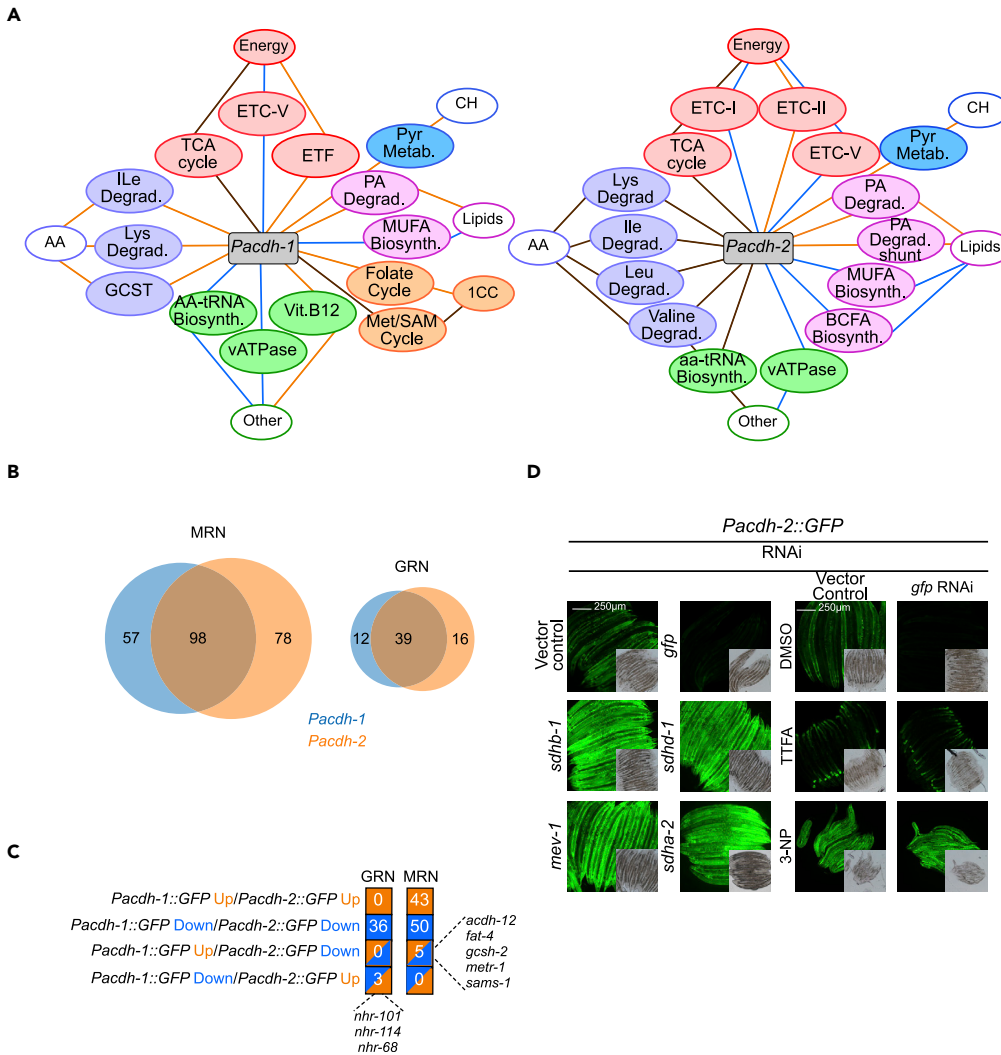


Figure 4. Comparison of regulation of *acd-1* and *acd-2* promoters

(A) Cartoons of enriched metabolic pathways regulating the *Pacdh-1::GFP* and *Pacdh-2::GFP* reporters.

(B) Venn diagrams of overlapping metabolic genes in the MRN (left) and TFs in the GRN (right) that regulate the *acd-1* and *acd-2* promoters.

(C) While many metabolic genes and TFs regulate both the *acd-1* and *acd-2* promoter, some have opposite effects.

(D) RNAi of ETC complex II members in the *Pacdh-2::GFP* reporter strain (left), ETC complex II inhibitory drug treatment (right, 125 μ M TTFA or 12.5 mM 3-NP), with or without GFP RNAi. The DMSO control relates to the TTFA panel. The control for 3-NP is shown in the upper panel of column 1. Related to Figure S4.

reduction of FAD to FADH₂, leading to the reduction of ubiquinone to ubiquinol in the mitochondrial membrane (Bezawork-Geleta et al., 2017). SDH is a complex of four subunits, each of which is encoded by a single gene in most organisms. *C. elegans*, however, has two close paralogs encoding the SDHA subunit: *sdha-1* and *sdha-2* (Rea and Johnson, 2003; Tsang and Lemire, 2003). Most subunits of SDH are essential for *C. elegans* development (Otero et al., 2019). However, there are viable mutants available for *sdha-2*, and RNAi of either paralog *sdha-1* or *sdha-2* activates the *acd-1* promoter (Figure 3B). Since ETC complex II-inhibiting drugs are not compatible with RNAi (Figure 4D), we crossed the *Pacdh-1::GFP* reporter into the *sdha-2(tm1420)* mutant to enable the identification of TFs that mediate the induction of gene expression in response to SDH perturbation. In *Pacdh-1::GFP;sdha-2(tm1420)* mutants, GFP fluorescence was increased compared to the wild-type background, validating the RNAi result (Figures 5A and 5B). In *Pacdh-1::GFP* reporter animals, GFP is completely shut off by diets high in vitamin B₁₂ or by direct vitamin B₁₂ supplementation (MacNeil et al., 2013; Watson et al., 2014) (Figure 5B). Interestingly, we

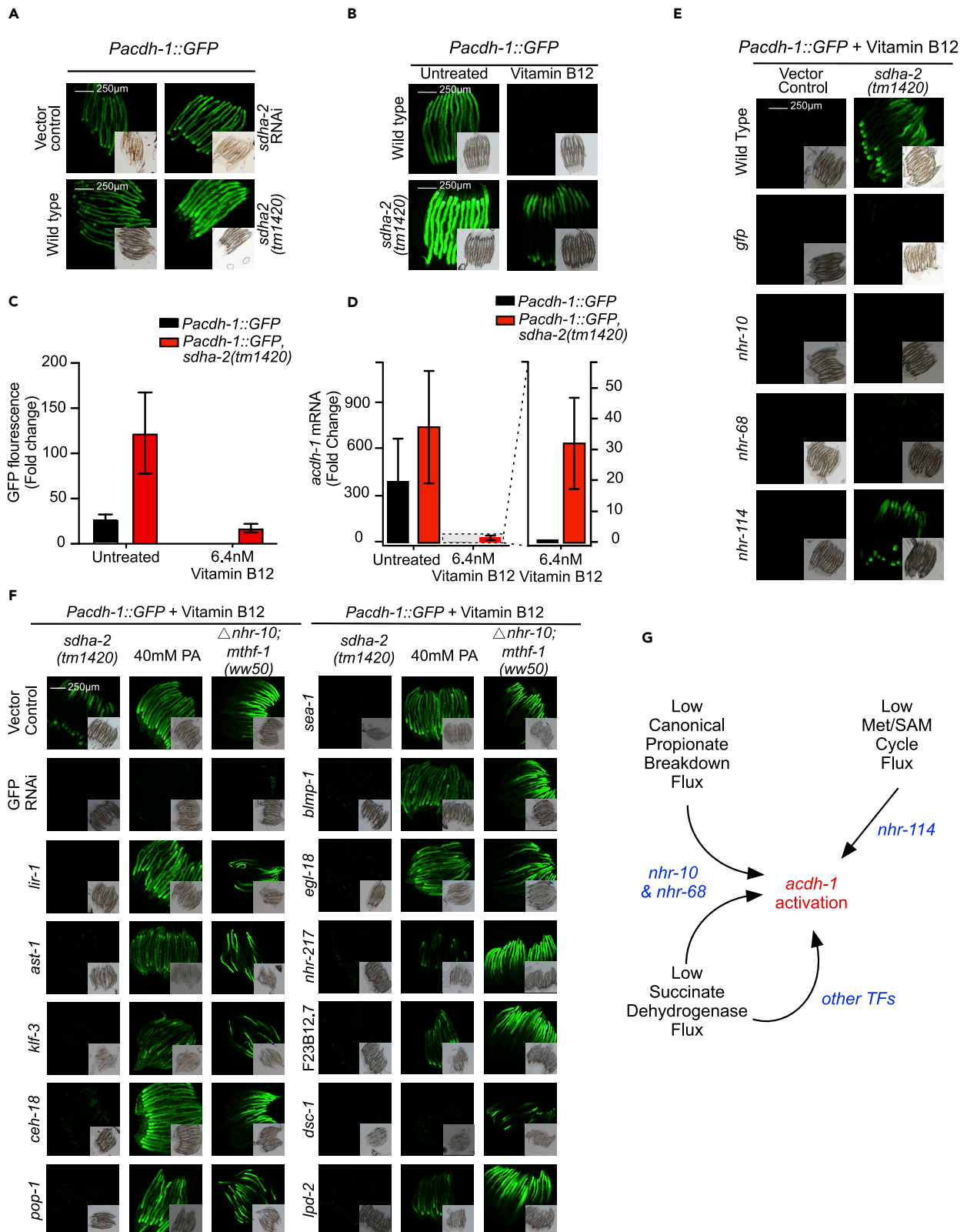


Figure 5. Transcriptional activation of *acdh-1* by ETC complex II inhibition

- (A) *Pacdh-1:GFP* animals exposed to *sdha-2* RNAi (top) or crossed into an *sdha-2(tm1420)* mutant (bottom).
 (B) *Pacdh-1:GFP* (wild type) and *Pacdh-1:GFP;sdha-2(tm1420)* animals with and without vitamin B₁₂ supplementation. Related to Figure S5.
 (C) Quantification of GFP in *Pacdh-1:GFP* animals with or without an *sdha-2* mutation and with or without vitamin B₁₂ supplementation.
 (D) qRT-PCR of endogenous *acdh-1* mRNA in wild type and *sdha-2* mutant animals with or without vitamin B₁₂ supplementation. Colors are as in (C). Data are represented as mean ± SD of three experimental repeats each containing three technical replicates. The mRNA fold changes were calculated with respect to *Pacdh-1:GFP* with added vitamin B₁₂.
 (E) *Pacdh-1:GFP;sdha-2(tm1420)* animals exposed to TF RNAi as indicated.
 (F) TF RNAi in *Pacdh-1:GFP* animals supplemented with vitamin B₁₂ and with an *sdha-2* mutation (left), exposed to propionate (low B₁₂ mechanism-I, middle) and with an *nhr-10* deletion and *mthf-1* mutation (low B₁₂ mechanism-II, right).
 (G) At least, three different, partially overlapping transcriptional mechanisms activate *acdh-1* expression in response to different metabolic perturbations.

found that vitamin B₁₂ supplementation did not fully repress GFP fluorescence either in the *sdha-2* mutant background, or in the presence of TTFA (Figures 5B and S5). However, GFP expression in the *sdha-2* mutant background with vitamin B₁₂ supplementation is lower than in wild-type animals without vitamin B₁₂. We quantified GFP induction in the reporter strain and endogenous *acdh-1* expression in the *sdha-2* mutant background, relative to the wild-type background, and both with and without supplementation of vitamin B₁₂ (Figures 5C and 5D). These results show that *acdh-1* is robustly induced by perturbations of ETC complex II, even in the presence of vitamin B₁₂ and indicate that this induction is distinct from *acdh-1* activation by perturbations in propionate degradation or dysregulation of the Met/SAM cycle, both of which can be suppressed by supplementation of vitamin B₁₂ (Bulcha et al., 2019; Giese et al., 2020).

Next, we asked which TFs mediate the activation of *acdh-1* expression in response to SDH perturbations. We first tested whether the TFs that mediate the response to low B₁₂ mechanisms I and II are also involved in the activation of the *acdh-1* promoter by SDH perturbation and found that, while RNAi of *nhr-114* (low B₁₂ mechanism-II) only mildly affected GFP levels, knockdown of either *nhr-10* or *nhr-68* (low B₁₂ mechanism-I) greatly reduced GFP expression (Figure 5E). This result shows that *nhr-68* and *nhr-10* mediate the activation of *acdh-1* not only in response to both excess propionate but also to SDH perturbation. As noted above, these mechanisms are, at least in part, distinct, since vitamin B₁₂ supplementation represses activation of *acdh-1* by excess propionate but not (fully) by SDH perturbation (Figure 5B). Therefore, we hypothesized that additional TFs may specifically be involved in the latter response. To test this hypothesis, we screened the TF RNAi library (MacNeil et al., 2015) in *Pacdh-1:GFP;sdha-2(tm1420)* animals in the presence of vitamin B₁₂. Altogether, we found multiple TFs that reduce GFP expression in these animals, some of which also lowered reporter expression in *Pacdh-1:GFP* animals that express GFP animals in response to low B₁₂ mechanism-I and, less frequently, low B₁₂ mechanism-II (Figure 5F). However, approximately half a dozen TFs are specific to SDH perturbations (Figure 5F). These results indicate that *acdh-1* activation in response to different metabolic perturbations is carried out by both overlapping and specific TFs (Figure 5G).

How does reduced flux through the SDH reaction activate *acdh-1* expression? We previously showed that *nhr-68* and *nhr-10* mediate activation of *acdh-1* expression in response to propionate accumulation (Bulcha et al., 2019). However, since several additional TFs specifically mediate the response to SDH perturbation, and because vitamin B₁₂ supplementation fails to fully repress the latter response, we hypothesized that SDH perturbation mediates its effect via other metabolic mechanisms. To test this hypothesis, we asked whether RNAi of other metabolic genes could specifically prevent the activation of *acdh-1* expression upon SDH perturbation. We performed RNAi of metabolic genes in *Pacdh-1:GFP;sdha-2(tm1420)* animals supplemented with vitamin B₁₂ using an expanded metabolic gene RNAi library (met-3.0) that includes ETC and other genes that were missed in the met-2.0 library (see STAR Methods). We screened for genes that specifically reduce GFP expression when knocked down in this mutant, i.e., that have little or no effect on the induction of *acdh-1* by low B₁₂ mechanisms-I or II. We identified genes that predominantly function in two metabolic pathways: the TCA cycle and the pentose phosphate pathway (PPP) (Figures 6A and 6B). Interestingly, the TCA cycle genes all function upstream of the generation of succinate, the substrate of the SDH complex, suggesting that succinate accumulation may result in *acdh-1* activation (Figure 6B). However, direct supplementation of succinate failed to induce *Pacdh-1:GFP*, but it is unclear whether succinate is taken up by the animal (data not shown). The contribution of the PPP to *acdh-1* activation by SDH perturbation also remains unclear. One intriguing possibility is that the generation of reducing agents NADPH by

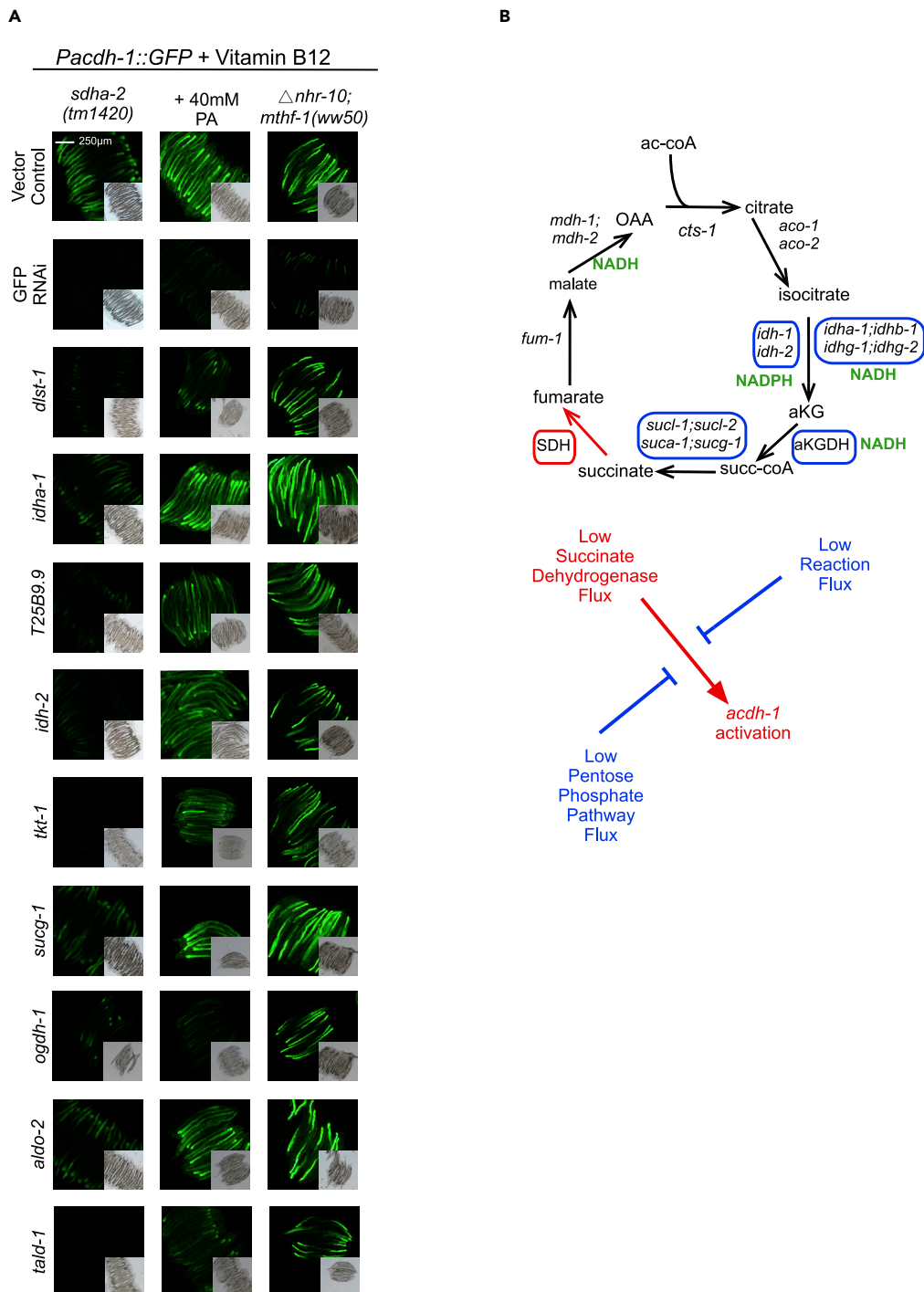


Figure 6. Inhibition of pentose phosphate pathway or TCA cycle flux suppresses activation of *acd-1* by ETC complex II inhibition

(A) Metabolic gene RNAi in *Pacdh-1::GFP* animals supplemented with vitamin B₁₂ and with an *sdha-2* mutation (left), exposed to propionate (low B₁₂ mechanism-I, middle) and with an *nhr-10* deletion and *mthf-1* mutation (low B₁₂ mechanism-II, right).

(B) Model of complex interactions among metabolic pathways regulating *acd-1* expression.

the PPP and NADH by the TCA cycle contributes to *acdH-1* activation, specifically in response to reduced flux in the SDH reaction. Altogether, these results reveal complex genetic interactions among metabolic pathways in the regulation of gene expression. Furthermore, the genetic analyses performed here show that *acdH-1* expression is modulated in response to additional metabolites in addition to propionate and SAM.

Transcription factors mediating the response to ETC complex III inhibition

Next, we explored the transcriptional mechanism that activates gene expression in response to another ETC component, ETC complex III. In contrast to ETC complex II inhibitors TTFA or 3-NP, both of which inhibit RNAi, supplementation with the ETC complex III inhibitor antimycin A did not interfere with RNAi; the drug induced intestinal activity of the *nhr-178* promoter and this induction was completely blocked by GFP RNAi (Figure 7A). To identify TFs involved in the response to ETC complex III inhibition, we screened the *Pnhr-178:GFP* reporter strain treated with antimycin A and found six TFs that, when knocked down by RNAi, blocked the activation of *Pnhr-178* promoter activity by antimycin A (Figure 7B). Two of these, *nhr-45* and *znf-207*, were found previously in the GRN and the proteins encoded by *nhr-45* and *sea-1* physically interact with the *Pnhr-178* promoter (Arda et al., 2010; Fuxman Bass et al., 2016; MacNeil et al., 2015).

We next focused on NHR-45 since it has been demonstrated to respond to mitochondrial dysfunction and because it physically binds the *nhr-178* promoter (Arda et al., 2010; Mao et al., 2019). We first used qRT-PCR to verify that both ETC complex III RNAi and antimycin A supplementation induced endogenous *nhr-178* expression, and that *nhr-45* is required for this induction (Figures 7C and 7D). Next, we asked whether the activation of *nhr-178* by *nhr-45* in response to ETC complex III perturbation had a functional consequence. Specifically, we asked whether *nhr-178* mutant animals are sensitive to antimycin A, as has been reported for *nhr-45* mutant animals (Mao et al., 2019). We confirmed that *nhr-45* mutant animals are much more sensitive to antimycin A than wild-type animals (Figure 7E). However, we did not observe a significant change in *nhr-178* mutant animals compared to wild-type animals; if anything, *nhr-178* mutant animals are slightly less sensitive to antimycin A (Figure 7E). Thus, the activation of *nhr-178* expression by *nhr-45* in response to ETC perturbation is not required to functionally mitigate the response to mitochondrial dysfunction.

Because both *nhr-45* and *nhr-178* are TFs (Reece-Hoyes et al., 2005), we wondered whether they share antimycin A-responsive target genes. We performed RNA-seq to identify genes that are induced by antimycin A and to determine which of those genes require *nhr-45*, *nhr-178*, both or neither. Because *nhr-45* mutant animals are very sensitive to antimycin A, we used a low dose of 0.3 μ M. In wild-type animals, 203 genes were differentially expressed by this dose of antimycin A; 163 were upregulated and 40 were downregulated (Figures 7F and S6; Tables S8 and S9). We used WormCat (Holdorf et al., 2020) and WormPaths (Walker et al., 2021) to ask whether any particular types of genes were induced by antimycin A treatment. We found an enrichment for genes involved in stress response and metabolism, specifically detoxification genes such as *ugt* and *cyp* genes, and genes involved in lipid metabolism. Induced genes include *cyp-14A4*, which was previously identified to be activated by antimycin A (Mao et al., 2019). Interestingly, we did not find induction of *nhr-178* by antimycin A, even though we could detect this activation by qRT-PCR (Figures 7C and 7D). This is probably because this gene is expressed at very low levels (0–1 TPM in wild-type animals) and/or due to the low dose of 0.3 μ M antimycin A used in this experiment. We found that of all 163 genes upregulated by antimycin A, 57 are dependent on *nhr-45*, 50 genes are dependent on *nhr-178*, 22 are dependent on both TFs, and 34 are dependent on neither TF (Figures 7G and S6; Table S8). Taken together, multiple TFs mediate the transcriptional activation of *nhr-178* by ETC complex III inhibition (Figure 7H). While *nhr-45* activates *nhr-178*, this is not required to mitigate lethality caused by ETC complex III inhibition, indicating that other *nhr-45* targets are required for this response and that *nhr-178* and its targets influence other transcriptional programs.

DISCUSSION

In this study, we show broad changes in intestinal promoter activity in response to metabolic gene RNAi and that certain types of metabolism, e.g., energy metabolism, more greatly affects promoter activity than other types of metabolism, e.g., carbohydrate metabolism. However, our promoter set is relatively small, and it remains to be determined whether this observation extends to the larger transcriptome. Here, it is important to note that the promoters were selected for our initial GRN study (MacNeil et al.,

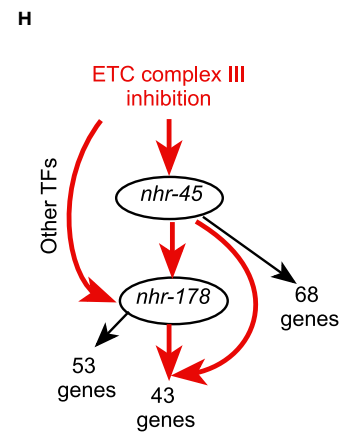
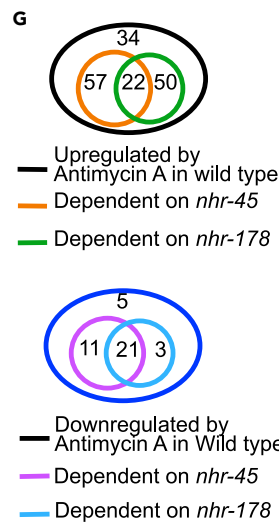
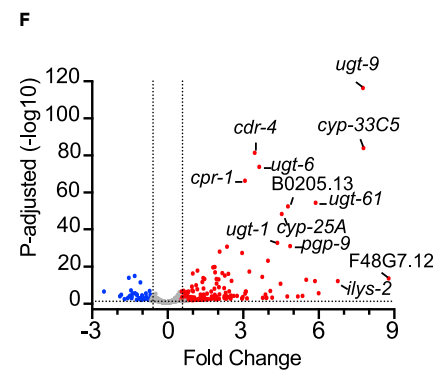
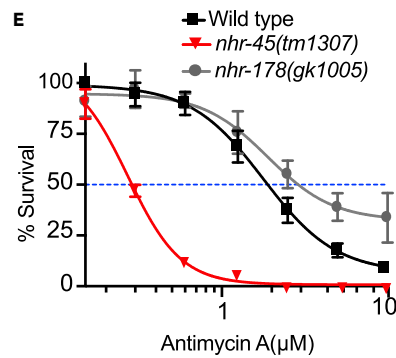
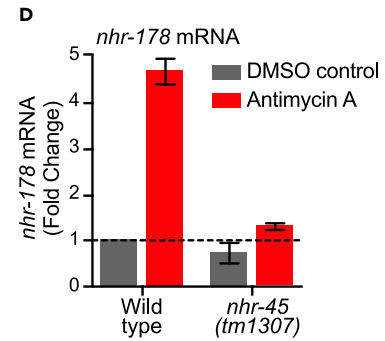
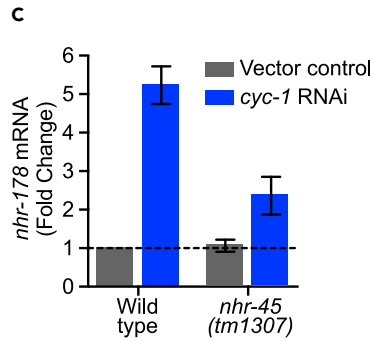
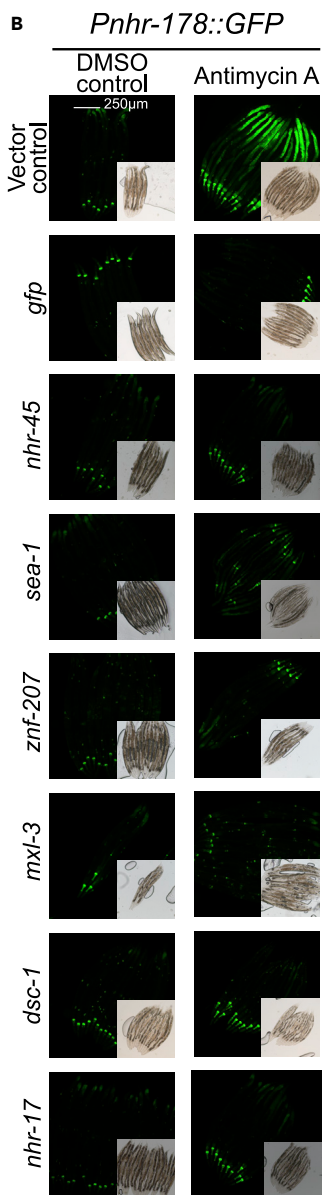
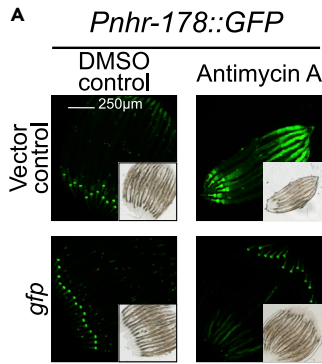


Figure 7. *nhr-45* and *nhr-178* together and independently regulate gene expression in response to ETC complex III inhibition

- (A) Antimycin A (0.3 μ M) supplementation to *Pnhr-178:GFP* reporter animals.
 (B) Examples of TFs that are required for the activation of the *nhr-178* promoter by antimycin A.
 (C) qRT-PCR of endogenous *nhr-178* with and without *cyc-1* RNAi in wild type and *nhr-45* mutant animals. Data are represented as mean \pm SD of three experimental repeats each containing three technical replicates. The mRNA fold changes were calculated with respect to wild type.
 (D) qRT-PCR of endogenous *nhr-178* with and without antimycin A supplementation in wild type and *nhr-45* mutant animals. Data are represented as mean \pm SD of three experimental repeats each containing three technical replicates. The mRNA fold changes were calculated with respect to untreated wild type.
 (E) Dose-response curve of antimycin A supplementation in wild type, *nhr-45* and *nhr-178* mutant animals. Data are represented as mean \pm SD of three experimental repeats each containing eight technical replicates.
 (F) Volcano plot of genes affected by antimycin A supplementation in wild-type animals measured by RNA-seq. Related to Tables S8 and S9.
 (G) Venn diagram of genes induced by antimycin A in wild-type animals that are dependent on *nhr-45*, *nhr-178*, both or neither. Related to Figure S6.
 (H) Cartoon of complex interplay between ETC complex III inhibition and transcriptional regulation.

2015) based on the fact that they drive expression in the *C. elegans* intestine, and that these promoters are not associated with any particular type of gene.

One of the main insights of this study is that metabolic gene knockdowns tend to activate gene expression. This contrasts with the RNAi of TFs, which tends to repress promoter activity (MacNeil et al., 2015). Altogether, these observations suggest that metabolic perturbations result in changes that are sensed, directly or indirectly, by TFs that induce promoter activity. Overall, we did not find great correlation between the number of metabolic genes and TFs that regulate each promoter, with the exception of the *acdh-1* and *acdh-2* promoters, which are affected by a large proportion of both metabolic gene and TF RNAi. For these promoters, this suggests that distinct TFs respond to different metabolic perturbations. We previously found that *acdh-1* expression is induced by different TFs for the response to low flux in the canonical propionate breakdown and the Met/SAM cycle, respectively (Bulcha et al., 2019; Giese et al., 2020). Here, we find that the *acdh-1* induction caused by SDH perturbations requires both TFs already known to regulate this gene in response to other perturbations, and TFs that are specific to this perturbation. We uncovered several additional pathways and complexes that activate *acdh-1* expression when perturbed, including pyruvate dehydrogenase (Table S3). We also found complex genetic interactions among metabolic pathways: activation of *acdh-1* expression by SDH perturbation, but not by propionate or low SAM, is blocked by simultaneous perturbation of genes that function upstream in the TCA cycle, or in the PPP. Future studies will determine how and why each pathway interacts with *acdh-1* expression and shed broader light on the connections between the MRN and the GRN and the transcriptional circuits involved.

We found that inhibition of the ETC affected the activity of many promoters tested. Surprisingly, we found different effects of different ETC complexes, indicating that the transcriptional response is not simply due to altered energy production. Instead, this finding suggests that perturbation of each complex may result in different metabolic changes that are sensed (directly or indirectly) by TFs that govern a transcriptional response. The effects of ETC complex RNAi were largely confirmed using ETC complex-inhibiting drugs. Remarkably, however, the two inhibitor drugs of ETC complex II, TTFA and 3-nitropropionate, show opposite effects on the *acdh-2* promoter, with 3-nitropropionate mimicking RNAi of most ETC complex II members. While these drugs have been reported to inhibit the same complex, they do not share the same mechanism of action. 3-nitropropionate is an analog of succinate, while TTFA binds the ubiquinone reaction site (Sun et al., 2005). Notably, 3-nitropropionate also inhibits isocitrate lyase, a key enzyme in the glyoxylate shunt (Schloss and Cleland, 1982). The differences in mechanism of action also cause separate changes in ETC complex II activity; while 3-nitropropionate irreversibly inhibits the entire complex, TTFA inhibits the succinate ubiquinone oxidoreductase activity of ETC complex II while leaving succinate dehydrogenase activity relatively intact (Guo et al., 2016; Lemarie et al., 2011). Our results indicate that these drugs induce non-overlapping metabolic changes that are sensed (directly or indirectly) by different TFs and can result in non-overlapping transcriptional changes. Therefore, these drugs may provide a tool to investigate the transcriptional mechanisms that respond to different mechanisms of ETC complex II inhibition in more detail, for instance using forward genetic screens and RNA-seq.

In this study, we used a gene-centered method to identify metabolic gene perturbations that modulate the activity of 19 promoters driving expression of a fluorescent protein in the *C. elegans* intestine. This method provides a complement to more widely used methods that use individual (metabolic) perturbations to measure genome-wide changes in metabolic gene expression by RNA-seq. There are advantages and disadvantages to our approach. Advantages include the fact that we examine a single tissue (the intestine), the ability to measure changes in promoters that drive the expression of lowly expressed genes for which

changes in gene expression are hard to confidently measure by RNA-seq (e.g., *nhr-178*), the ability to trace a regulatory effect to a specific genomic DNA element (the promoter), and the testing of genome-scale perturbations of metabolism. Disadvantages include the relatively high level of noise in the primary screen, and the fact that RNAi does not work equally well in all *C. elegans* tissues (Kamath et al., 2001; Timmons et al., 2001). However, this is offset, at least in part, by the fact that metabolism can be analyzed at the level of pathways, which provides a degree of confidence in the observations. However, a lack of pathway enrichment does not necessarily mean the interactions are false. Overall, we strived to be stringent in the experiments. Therefore, we suspect that we have missed more interactions (false negatives) than called wrong interactions (false positives). Other disadvantages of our approach include the fact that our experiments are qualitative rather than quantitative because we visually assess changes in promoter activity. Since we only specifically aimed to identify changes in fluorescent protein levels in the intestine, and because 18 of the 19 reporter strains also express the fluorescent protein in other tissues, it was not feasible to automate the scoring using imaging or by a plate reader, both of which we have used previously (Bulcha et al., 2019; Mori et al., 2017).

Taken together, our study provides a first glimpse in the complex interactions between GRNs and MRNs and sets the stage for incorporating additional types of networks by performing RNAi with additional types of genes, including those encoding transcriptional cofactors, RNA binding proteins, and signaling factors to obtain an integrative view on promoter regulation in an animal.

Limitations of the study

Large-scale visual RNAi screens can be inefficient and noisy. For example, the variation in the brightness of the reporters, some of which are relatively faint, can lead to false negatives. Additionally, the reporter constructs used in the study contain isolated promoter regions that have been taken out of their normal chromosomal context and may not accurately represent endogenous gene expression.

STAR★METHODS

Detailed methods are provided in the online version of this paper and include the following:

- KEY RESOURCES TABLE
- RESOURCE AVAILABILITY
 - Lead contact
 - Materials availability
 - Data and code availability
- EXPERIMENTAL MODEL AND SUBJECT DETAILS
 - *C. elegans*
- METHOD DETAILS
 - Metabolic gene RNAi libraries
 - *C. elegans* RNAi assays
 - Metabolic pathway enrichment analysis
 - Drug treatment
 - Bacterial growth assays with TTFA
 - GFP quantification
 - qRT-PCR
 - Expression profiling by RNA-seq
 - Antimycin toxicity assay
 - Sequence alignment
- QUANTIFICATION AND STATISTICAL ANALYSIS

SUPPLEMENTAL INFORMATION

Supplemental information can be found online at <https://doi.org/10.1016/j.isci.2022.104688>.

ACKNOWLEDGEMENTS

We thank members of the Walhout lab, Job Dekker, Safak Yilmaz, and Olga Ponomarova for discussion and critical reading of the manuscript. We thank Gustavo Salinas for the *sdha-2(tm1420)* strain. This work was supported by a grant from the National Institutes of Health R35GM122502 to A.J.M.W. Some nematode

strains used in this work were provided by the CGC, which is funded by the NIH Office of Research Infrastructure Programs (P40 OD010440).

AUTHOR CONTRIBUTIONS

S.B. and A.J.M.W. conceived the study. S.B. performed most experiments with help from B.B.H. (FFL analysis, qRT-PCR, and sequence alignment), H.Z. (RNA-seq library preparation), X.L. (RNA-seq analysis), and G.E.G. (bacterial growth assays). The met-2.0 RNAi library was generated by J.Z. Pathway analysis was done by A.D.H. The paper was written by A.J.M.W. and A.D.H. with editing by all other authors.

DECLARATION OF INTERESTS

The authors declare no competing interests.

Received: April 28, 2022

Revised: June 12, 2022

Accepted: June 24, 2022

Published: August 19, 2022

SUPPORTING CITATIONS

The following references appear in the Supplemental information: [Bolz et al. 2010](#); [Calfon et al., 2002](#); [Grove et al., 2009](#); [Libina et al., 2003](#); [Liu et al., 2009](#); [Martinez et al., 2008](#); [Murray et al., 2012](#); [Tawe et al., 1998](#).

REFERENCES

- Alston, T.A., Mela, L., and Bright, H.J. (1977). 3-Nitropropionate, the toxic substance of *Indigofera*, is a suicide inactivator of succinate dehydrogenase. *Proc. Natl. Acad. Sci. USA* **74**, 3767–3771. <https://doi.org/10.1073/pnas.74.9.3767>.
- Arda, H.E., Taubert, S., MacNeil, L.T., Conine, C.C., Tsuda, B., Van Gilst, M., Sequerra, R., Doucette-Stamm, L., Yamamoto, K.R., and Walhout, A.J.M. (2010). Functional modularity of nuclear hormone receptors in a *C. elegans* gene regulatory network. *Mol. Syst. Biol.* **6**, 367. <https://doi.org/10.1038/msb.2010.23>.
- Armson, A., Grubb, W.B., and Mendis, A. (1995). The effect of electron transport (ET) inhibitors and thiabendazole on the fumarate reductase (FR) and succinate dehydrogenase (SDH) of *Strongyloides ratti* infective (L3) larvae. *Int. J. Parasitol.* **25**, 261–263. [https://doi.org/10.1016/0020-7519\(94\)e0061-q](https://doi.org/10.1016/0020-7519(94)e0061-q).
- Bezawork-Geleta, A., Rohlena, J., Dong, L., Pacak, K., and Neuzil, J. (2017). Mitochondrial complex II: at the crossroads. *Trends Biochem. Sci.* **42**, 312–325. <https://doi.org/10.1016/j.tibs.2017.01.003>.
- Bolz, D.D., Tenor, J.L., and Aballay, A. (2010). A conserved PMK-1/p38 MAPK is required in *Caenorhabditis elegans* tissue-specific immune response to *Yersinia pestis* infection. *J. Biol. Chem.* **285**, 10832–10840. <https://doi.org/10.1074/jbc.M109.091629>.
- Brenner, S. (1974). The genetics of *Caenorhabditis elegans*. *Genetics* **77**, 71–94. <https://doi.org/10.1093/genetics/77.1.71>.
- Bulcha, J.T., Giese, G.E., Ali, M.Z., Lee, Y.-U., Walker, M.D., Holdorf, A.D., Yilmaz, L.S., Brewster, R.C., and Walhout, A.J. (2019). A persistence detector for metabolic network rewiring in an animal. *Cell Rep.* **26**, 460–468.e4. <https://doi.org/10.1016/j.celrep.2018.12.064>.
- Calfon, M., Zeng, H., Urano, F., Till, J.H., Hubbard, S.R., Harding, H.P., Clark, S.G., and Ron, D. (2002). IRE1 couples endoplasmic reticulum load to secretory capacity by processing the XBP-1 mRNA. *Nature* **415**, 92–96. <https://doi.org/10.1038/415092a>.
- Cao, J., Packer, J.S., Ramani, V., Cusanovich, D.A., Huynh, C., Daza, R., Qiu, X., Lee, C., Furlan, S.N., Steemers, F.J., et al. (2017). Comprehensive single-cell transcriptional profiling of a multicellular organism. *Science* **357**, 661–667. <https://doi.org/10.1126/science.aam8940>.
- Conte, D., Jr., MacNeil, L.T., Walhout, A.J.M., and Mello, C.C. (2015). RNA interference in *Caenorhabditis elegans*. *Curr. Protoc. Mol. Biol.* **109**, 26.3.1–26.3.30. <https://doi.org/10.1002/0471142727.mb2603s109>.
- Edgar, R.C. (2004). MUSCLE: multiple sequence alignment with high accuracy and high throughput. *Nucleic Acids Res.* **32**, 1792–1797. <https://doi.org/10.1093/nar/gkh340>.
- Fuxman Bass, J.I., Pons, C., Kozlowski, L., Reece-Hoyes, J.S., Shrestha, S., Holdorf, A.D., Mori, A., Myers, C.L., and Walhout, A.J. (2016). A gene-centered *C. elegans* protein-DNA interaction network provides a framework for functional predictions. *Mol. Syst. Biol.* **12**, 884. <https://doi.org/10.15252/msb.20167131>.
- Gerstein, M.B., Lu, Z.J., Van Nostrand, E.L., Cheng, C., Arshinoff, B.I., Liu, T., Yip, K.Y., Robilotto, R., Rechtsteiner, A., Ikegami, K., et al. (2010). Integrative analysis of the *Caenorhabditis elegans* genome by the modENCODE project. *Science* **330**, 1775–1787. <https://doi.org/10.1126/science.1196914>.
- Giese, G.E., Walker, M.D., Ponomarova, O., Zhang, H., Li, X., Minevich, G., and Walhout, A.J. (2020). *Caenorhabditis elegans* methionine/S-adenosylmethionine cycle activity is sensed and adjusted by a nuclear hormone receptor. *Elife* **9**, e60259. <https://doi.org/10.7554/elifesc60259>.
- Gilbert, W., and Müller-Hill, B. (1966). Isolation of the lac repressor. *Proc. Natl. Acad. Sci. USA* **56**, 1891–1898. <https://doi.org/10.1073/pnas.56.6.1891>.
- Goedhart, J., and Luijsterburg, M.S. (2020). VolcanoR is a web app for creating, exploring, labeling and sharing volcano plots. *Sci Rep* **10**, 20560. <https://doi.org/10.1038/s41598-020-76603-3>.
- Grove, C.A., deMasi, F., Barrasa, M.I., Newburger, D.E., Alkema, M.J., Bulyk, M.L., and Walhout, A.J. (2009). A multiparameter network reveals extensive divergence between *C. elegans* bHLH transcription factors. *Cell* **138**, 314–327. <https://doi.org/10.1016/j.cell.2009.04.058>.
- Guo, L., Shestov, A.A., Worth, A.J., Nath, K., Nelson, D.S., Leeper, D.B., Glickson, J.D., and Blair, I.A. (2016). Inhibition of mitochondrial complex II by the anticancer agent Isonitazene. *J. Biol. Chem.* **291**, 42–57. <https://doi.org/10.1074/jbc.M115.697516>.
- Hashimshony, T., Senderovich, N., Avital, G., Klochender, A., de Leeuw, Y., Anavy, L., Gennert, D., Li, S., Livak, K.J., Rozenblatt-Rosen, O., et al. (2016). CEL-Seq2: sensitive highly-multiplexed single-cell RNA-Seq. *Genome Biol.* **17**, 77. <https://doi.org/10.1186/s13059-016-0938-8>.
- Holdorf, A.D., Higgins, D.P., Hart, A.C., Boag, P.R., Pazour, G.J., Walhout, A.J.M., and Walker, A.K. (2020). WormCat: an online tool for annotation and visualization of *Caenorhabditis elegans* genome-scale data. *Genetics* **214**, 279–294. <https://doi.org/10.1534/genetics.119.302919>.
- Hong, S., and Pedersen, P.L. (2008). ATP synthase and the actions of inhibitors utilized to study its roles in human health, disease, and other scientific

- areas. *Microbiol. Mol. Biol. Rev.* 72, 590–641. <https://doi.org/10.1128/mmlbr.00016-08>.
- Ideker, T., Thorsson, V., Ranish, J.A., Christmas, R., Buhler, J., Eng, J.K., Bumgarner, R., Goodlett, D.R., Aebersold, R., and Hood, L. (2001). Integrated genomic and proteomic analyses of a systematically perturbed metabolic network. *Science* 292, 929–934. <https://doi.org/10.1126/science.292.5518.929>.
- Jacob, F., and Monod, J. (1961). Genetic regulatory mechanisms in the synthesis of proteins. *J. Mol. Biol.* 3, 318–356. [https://doi.org/10.1016/s0022-2836\(61\)80072-7](https://doi.org/10.1016/s0022-2836(61)80072-7).
- Johnston, M. (1987). A model fungal gene regulatory mechanism: the GAL genes of *Saccharomyces cerevisiae*. *Microbiol. Rev.* 51, 458–476. <https://doi.org/10.1128/mr.51.4.458-476.1987>.
- Kamath, R.S., Martinez-Campos, M., Zipperlen, P., Fraser, A.G., and Ahringer, J. (2001). Effectiveness of specific RNA-mediated interference through ingested double-stranded RNA in *Caenorhabditis elegans*. *Genome Biol.* 2, RESEARCH0002. <https://doi.org/10.1186/gb-2000-2-1-research0002>.
- Kamath, R.S., Fraser, A.G., Dong, Y., Poulin, G., Durbin, R., Gotta, M., Kanapin, A., Le Bot, N., Moreno, S., Sohrmann, M., et al. (2003). Systematic functional analysis of the *Caenorhabditis elegans* genome using RNAi. *Nature* 421, 231–237. <https://doi.org/10.1038/nature01278>.
- Lemarie, A., Huc, L., Pazarentzos, E., Mahul-Mellier, A.L., and Grimm, S. (2011). Specific disintegration of complex II succinate:ubiquinone oxidoreductase links pH changes to oxidative stress for apoptosis induction. *Cell Death Differ.* 18, 338–349. <https://doi.org/10.1038/cdd.2010.93>.
- Libina, N., Berman, J.R., and Kenyon, C. (2003). Tissue-specific activities of *C. elegans* DAF-16 in the regulation of lifespan. *Cell* 115, 489–502. [https://doi.org/10.1016/s0092-8674\(03\)00889-4](https://doi.org/10.1016/s0092-8674(03)00889-4).
- Liu, X., Long, F., Peng, H., Aerni, S.J., Jiang, M., Sánchez-Blanco, A., Murray, J.I., Preston, E., Mericle, B., Batzoglou, S., et al. (2009). Analysis of cell fate from single-cell gene expression profiles in *C. elegans*. *Cell* 139, 623–633. <https://doi.org/10.1016/j.cell.2009.08.044>.
- Livak, K.J., and Schmittgen, T.D. (2001). Analysis of relative gene expression data using real-time quantitative PCR and the 2^{-ΔΔCT} method. *Methods* 25, 402–408. <https://doi.org/10.1006/meth.2001.1262>.
- MacNeil, L., Watson, E., Arda, H., Zhu, L., and Walhout, A. (2013). Diet-induced developmental acceleration independent of TOR and insulin in *C. elegans*. *Cell* 153, 240–252. <https://doi.org/10.1016/j.cell.2013.02.049>.
- MacNeil, L., Pons, C., Arda, H., Giese, G., Myers, C., and Walhout, A. (2015). Transcription factor Activity mapping of a tissue-specific In Vivo gene regulatory network. *Cell Syst.* 1, 152–162. <https://doi.org/10.1016/j.cels.2015.08.003>.
- Mangan, S., and Alon, U. (2003). Structure and function of the feed-forward loop network motif. *Proc. Natl. Acad. Sci. USA* 100, 11980–11985. <https://doi.org/10.1073/pnas.2133841100>.
- Mao, K., Ji, F., Breen, P., Sewell, A., Han, M., Sadreyev, R., and Ruvkun, G. (2019). Mitochondrial dysfunction in *C. elegans* activates mitochondrial relocalization and nuclear hormone receptor-dependent detoxification genes. *Cell Metab.* 29, 1182–1191.e4. <https://doi.org/10.1016/j.cmet.2019.01.022>.
- Martinez, N.J., Ow, M.C., Reece-Hoyes, J.S., Barrasa, M.I., Ambros, V.R., and Walhout, A.J. (2008). Genome-scale spatiotemporal analysis of *Caenorhabditis elegans* microRNA promoter activity. *Genome Res.* 18, 2005–2015. <https://doi.org/10.1101/gr.083055.108>.
- McGhee, J.D. (2007). The *C. elegans* Intestine (Wormbook). www.wormbook.org.
- Melo, J., and Ruvkun, G. (2012). Inactivation of conserved *C. elegans* genes engages pathogen- and xenobiotic-associated defenses. *Cell* 149, 452–466. <https://doi.org/10.1016/j.cell.2012.02.050>.
- Mori, A., Holdorf, A.D., and Walhout, A.J. (2017). Many transcription factors contribute to *C. elegans* growth and fat storage. *Genes Cells* 22, 770–784. <https://doi.org/10.1111/gtc.12516>.
- Murray, J.I., Boyle, T.J., Preston, E., Vafeados, D., Mericle, B., Weisdepp, P., Zhao, Z., Bao, Z., Boeck, M., and Waterston, R.H. (2012). Multidimensional regulation of gene expression in the *C. elegans* embryo. *Genome Res.* 22, 1282–1294. <https://doi.org/10.1101/gr.131920.111>.
- Nigon, V.M., and Felix, M.A. (2017). History of research on *C. elegans* and other free-living nematodes as model organisms. *WormBook* 2017, 1–84. <https://doi.org/10.1895/wormbook.1.181.1>.
- Otero, L., Martínez-Rosales, C., Barrera, E., Pantano, S., and Salinas, G. (2019). Complex I and II subunit gene duplications provide increased fitness to worms. *Front. Genet.* 10, 1043. <https://doi.org/10.3389/fgene.2019.01043>.
- Packer, J.S., Zhu, Q., Huynh, C., Sivaramakrishnan, P., Preston, E., Dueck, H., Stefanik, D., Tan, K., Trapnell, C., Kim, J., et al. (2019). A lineage-resolved molecular atlas of *C. elegans* embryogenesis at single-cell resolution. *Science* 365, eaax1971. <https://doi.org/10.1126/science.aax1971>.
- Palmer, G., Horgan, D.J., Tisdale, H., Singer, T.P., and Beinert, H. (1968). Studies on the respiratory chain-linked reduced nicotinamide adenine dinucleotide dehydrogenase. XIV. Location of the sites of inhibition of rotenone, barbiturates, and piericidin by means of electron paramagnetic resonance spectroscopy. *J. Biol. Chem.* 243, 844–847. [https://doi.org/10.1016/s0021-9258\(19\)81742-8](https://doi.org/10.1016/s0021-9258(19)81742-8).
- Rea, S., and Johnson, T.E. (2003). A metabolic model for life span determination in *Caenorhabditis elegans*. *Dev. Cell* 5, 197–203. [https://doi.org/10.1016/s1534-5807\(03\)00242-9](https://doi.org/10.1016/s1534-5807(03)00242-9).
- Reece-Hoyes, J.S., Deplancke, B., Shingles, J., Grove, C.A., Hope, I.A., and Walhout, A.J.M. (2005). A compendium of *C. elegans* regulatory transcription factors: a resource for mapping transcription regulatory networks. *Genome Biol.* 6, R110. <https://doi.org/10.1186/gb-2005-6-13-r110>.
- Rual, J.-F., Ceron, J., Koreth, J., Hao, T., Nicot, A.-S., Hirozane-Kishikawa, T., Vandenhaute, J., Orkin, S.H., Hill, D.E., van den Heuvel, S., and Vidal, M. (2004). Toward improving *Caenorhabditis elegans* phenome mapping with an ORFeome-based RNAi library. *Genome Res.* 14, 2162–2168. <https://doi.org/10.1101/gr.2505604>.
- Rubio Gomez, M.A., and Ibba, M. (2020). Aminoacyl-tRNA synthetases. *RNA* 26, 910–936. <https://doi.org/10.1261/ma.071720.119>.
- Schloss, J.V., and Cleland, W.W. (1982). Inhibition of isocitrate lyase by 3-nitropropionate, a reaction-intermediate analogue. *Biochemistry* 21, 4420–4427. <https://doi.org/10.1021/bi00261a035>.
- Slater, E.C. (1973). The mechanism of action of the respiratory inhibitor, antimycin. *Biochim. Biophys. Acta* 301, 129–154. [https://doi.org/10.1016/0304-4173\(73\)90002-5](https://doi.org/10.1016/0304-4173(73)90002-5).
- Stannard, J.N., and Horecker, B.L. (1947). The in vitro inhibition of cytochrome oxidase by azide and cyanide. *Fed. Proc.* 6, 210.
- Sun, F., Huo, X., Zhai, Y., Wang, A., Xu, J., Su, D., Bartlam, M., and Rao, Z. (2005). Crystal structure of mitochondrial respiratory membrane protein complex II. *Cell* 121, 1043–1057. <https://doi.org/10.1016/j.cell.2005.05.025>.
- Tamura, K., Stecher, G., and Kumar, S. (2021). MEGA11: molecular evolutionary genetics analysis version 11. *Mol. Biol. Evol.* 38, 3022–3027. <https://doi.org/10.1093/molbev/msab120>.
- Tawe, W.N., Eschbach, M.L., Walter, R.D., and Henkle-Duhrsen, K. (1998). Identification of stress-responsive genes in *Caenorhabditis elegans* using RT-PCR differential display. *Nucleic Acids Res.* 26, 1621–1627. <https://doi.org/10.1093/nar/26.7.1621>.
- Timmons, L., Court, D.L., and Fire, A. (2001). Ingestion of bacterially expressed dsRNAs can produce specific and potent genetic interference in *Caenorhabditis elegans*. *Gene* 263, 103–112. [https://doi.org/10.1016/s0378-1119\(00\)00579-5](https://doi.org/10.1016/s0378-1119(00)00579-5).
- Tsang, W.Y., and Lemire, B.D. (2003). The role of mitochondria in the life of the nematode, *Caenorhabditis elegans*. *Biochim. Biophys. Acta* 1638, 91–105. [https://doi.org/10.1016/s0925-4439\(03\)00079-6](https://doi.org/10.1016/s0925-4439(03)00079-6).
- Van Nostrand, E.L., and Kim, S.K. (2013). Integrative analysis of *C. elegans* modENCODE ChIP-seq data sets to infer gene regulatory interactions. *Genome Res.* 23, 941–953. <https://doi.org/10.1101/gr.152876.112>.
- Walker, M.D., Giese, G.E., Holdorf, A.D., Bhattacharya, S., Diot, C., Garcia-Gonzalez, A.P., Horowitz, B.B., Lee, Y.U., Leland, T., Li, X., et al. (2021). WormPaths: *Caenorhabditis elegans* metabolic pathway annotation and visualization. *Genetics* 219, iyab089.

Wang, X., Sato, R., Brown, M.S., Hua, X., and Goldstein, J.L. (1994). SREBP-1, a membrane-bound transcription factor released by sterol-regulated proteolysis. *Cell* 77, 53–62. [https://doi.org/10.1016/0092-8674\(94\)90234-8](https://doi.org/10.1016/0092-8674(94)90234-8).

Watson, E., and Walhout, A.J. (2014). *Caenorhabditis elegans* metabolic gene regulatory networks govern the cellular economy. *Trends Endocrinol. Metab.* 25, 502–508. <https://doi.org/10.1016/j.tem.2014.03.004>.

Watson, E., MacNeil, L., Arda, H., Zhu, L., and Walhout, A. (2013). Integration of metabolic and gene regulatory networks modulates the *C. elegans* dietary response. *Cell* 153, 253–266. <https://doi.org/10.1016/j.cell.2013.05.022>.

Watson, E., MacNeil, L., Ritter, A., Yilmaz, L., Rosebrock, A., Caudy, A., and Walhout, A. (2014). Interspecies systems biology uncovers metabolites affecting *C. elegans* gene expression and life history traits. *Cell* 156, 759–770. <https://doi.org/10.1016/j.cell.2014.01.047>.

Watson, E., Olin-Sandoval, V., Hoy, M.J., Li, C.-H., Louisse, T., Yao, V., Mori, A., Holdorf, A.D., Troyanskaya, O.G., Ralser, M., and Walhout, A.J. (2016). Metabolic network rewiring of propionate flux compensates vitamin B12 deficiency in *C. elegans*. *Elife* 5, e17670. <https://doi.org/10.7554/elife.17670>.

Watts, J.L., and Ristow, M. (2017). Lipid and carbohydrate metabolism in *Caenorhabditis elegans*. *Genetics* 207, 413–446. <https://doi.org/10.1534/genetics.117.300106>.

Yilmaz, L., and Walhout, A. (2016). A *Caenorhabditis elegans* genome-scale metabolic network model. *Cell Syst.* 2, 297–311. <https://doi.org/10.1016/j.cels.2016.04.012>.

Yilmaz, L.S., Li, X., Nanda, S., Fox, B., Schroeder, F., and Walhout, A.J. (2020). Modeling tissue-relevant *Caenorhabditis elegans* metabolism at network, pathway, reaction, and metabolite levels. *Mol. Syst. Biol.* 16, e9649. <https://doi.org/10.15252/msb.20209649>.

Yokoyama, C., Wang, X., Briggs, M.R., Admon, A., Wu, J., Hua, X., Goldstein, J.L., and Brown, M.S. (1993). SREBP-1, a basic-helix-loop-helix-leucine zipper protein that controls transcription of the low density lipoprotein receptor gene. *Cell* 75, 187–197. [https://doi.org/10.1016/s0092-8674\(05\)80095-9](https://doi.org/10.1016/s0092-8674(05)80095-9).

STAR★METHODS

KEY RESOURCES TABLE

REAGENT or RESOURCE	SOURCE	IDENTIFIER
Bacterial and virus strains		
<i>Escherichia coli</i> OP50	Caenorhabditis Genetics N/A Center (CGC)	N/A
<i>Escherichia coli</i> HT115	CGC	N/A
<i>Escherichia coli</i> HT115 Ahringer RNAi Library	Kamath et al. (2003)	N/A
<i>Escherichia coli</i> HT115 ORFeome RNAi Library	Rual et al. (2004)	N/A
Chemicals, peptides, and recombinant proteins		
Propionic Acid	Sigma Aldrich	Cat#: P1386
Isopropyl b-D-1 thiogalactopyranoside (IPTG)	US Biological	Cat#: I8500
Levamisole Hydrochloride	Sigma Aldrich	Cat#: PHR1798
TRizol Reagent	Life Technologies	Cat#: 15596-018
M-MuLV Reverse Transcriptase	NEB	Cat#: M0253
Direct-zol RNA Mini Prep Kit	Zymo Research	Cat#: R2050
DNase I	NEB	Cat#: M0303
Oligo(dT) 12–18 Primer	Invitrogen	Cat#: 18418012
RNaseOut	Invitrogen	Cat#: 10777019
Fast SYBR Green Master Mix	ThermoFisher Scientific	Cat#: 4385616
Antimycin A	Sigma Aldrich	Cat#: A8674
2-Thenoyltri-fluoroacetone (TTFA)	Sigma Aldrich	Cat#: T27006
Rotenone	Sigma Aldrich	Cat#: R8875
Sodium Azide	Sigma Aldrich	Cat#: S2002
DMSO	Sigma Aldrich	Cat#: D8418
Vitamin B ₁₂	Sigma Aldrich	Cat#: V2876
Deposited data		
Raw and analyzed RNA-seq data	This study	GEO: GSE19433
Experimental models: Organisms/strains		
<i>Caenorhabditis elegans</i> N2 (wild type)	CGC/NBRP	N/A
<i>C. elegans</i> (sdha-2 (tm1420) I)	National Bioresource Worm Base Project, Japan	Wormbase: WBVar00250413
<i>C. elegans</i> , sdha-2(tm1420); wwls24[Pacdh-1:: GFP; unc-119(+)]	This study	Strain: VL1458
<i>C. elegans</i> , (wwls24[Pacdh-1:: GFP; unc-119(+)]; nhr-10(tm4695); mthf- 1(ww50)	Giese et al. (2020)	VL1199, WBStrain00049238
nhr-45(tm1307) X	Arda et al. (2010)	VL484, WBStrain00040126
nhr-45(tm1307), Pnhr-178::GFP	Arda et al. (2010)	VL739, WBStrain00040154
nhr-178(gk1005) V	Fuxman Bass et al. (2016)	VL1135
Oligonucleotides		
List of Oligonucleotides	This study	Table S11
Software and algorithms		
Graphic	Graphic Pita Inc.	Graphic.com
Bio-render	Biorender.com	Biorender (RRID:SCR_018361)

(Continued on next page)

Continued

REAGENT or RESOURCE	SOURCE	IDENTIFIER
Graph Pad Prism 9	Graph Pad	GraphPad Prism (RRID:SCR_002798)
VolcaNoseR	Goedhart and Luijsterburg, 2020	https://huygens.science.uva.nl/VolcaNoseR
Step One Plus qPCR Software v2.3	Thermo Fisher Scientific	Cat#: 4376600, RRID:SCR_014281
DESeq2	Bioconductor	https://doi.org/10.18129/B9.bioc.DESeq2 DESeq2 (RRID:SCR_015687)
MEGA11, MUSCLE algorithm	Tamura et al. (2021) , Edgar (2004)	https://www.megasoftware.net/ , MEGA Software (RRID:SCR_000667), MUSCLE (RRID:SCR_011812)
Cytoscape	Cytoscape- 3.9.1	Cytoscape (RRID:SCR_003032)

RESOURCE AVAILABILITY

Lead contact

Further information and requests for reagents may be directed to and will be fulfilled by the lead contact Albertha J.M. Walhout (marian.walhout@umassmed.edu).

Materials availability

All new and unique reagents generated in this study will be made available by the [Lead contact](#) without restriction.

Data and code availability

- The RNAseq data has been deposited in the National Center for Biotechnology Information Gene Expression Omnibus database (GEO: GSE19433).
- This paper does not report original code
- Any additional information required to reanalyze the data reported in this paper is available from the [Lead contact](#) upon request.

EXPERIMENTAL MODEL AND SUBJECT DETAILS

C. elegans

N2 (Bristol) was used as the wild-type strain, and animals were maintained with *E. coli* OP50 as diet on Nematode Growth Media (NGM), as previously described ([Brenner, 1974](#)). The 19 reporter strains are multi-copy transgenes, some of which are integrated in the genome. Details are described in our previous study ([MacNeil et al., 2015](#)). The *nhr-178(gk1005) V* and *nhr-45(tm1307) X*, mutants were provided by *Caenorhabditis* Genetics Center (CGC), and the *sdha-2 (tm1420) I*, mutant was generously provided by Gustavo Salinas, who received it from the National Bioresource Project, Japan. All mutant strains were backcrossed three times to N2 animals. VL1199(*wwls24[Pacdh-1::GFP;unc-119(+);nhr-10(tm4695);mthf-1(ww50)*) has been described previously ([Giese et al., 2020](#)).

METHOD DETAILS

Metabolic gene RNAi libraries

We previously generated an RNAi library of 836 metabolic genes that were curated based on KEGG and Wormbase descriptions ([Watson et al., 2016](#)). We removed genes that were not relevant (e.g., polymerases) and added metabolic genes defined by iCEL1273, our reconstructed genome-scale metabolic network model ([Yilmaz and Walhout, 2016](#)). We also added 257 genes that have high homology with at least one metabolic enzyme in other organisms, some of which are included in our more recent iCEL1314 model ([Yilmaz et al., 2020](#)). We then removed duplicates, transposons, pseudogenes, and clones that sequenced incorrectly for a final of 1,495 unique metabolic genes. Available RNAi clones were obtained from the ORFeome ([Rual et al., 2004](#)) and Ahringer RNAi collections ([Kamath et al., 2003](#)), and arrayed in 96-well plates. This library is referred to as met-2.0 and was used in the primary screen ([Table S1](#)). For the screen with the *Pacdh-1::GFP;sdha-2(tm1420)* mutant, we expanded the library by adding ETC genes and

additional genes that were missed in the met-2.0 library, and included vector, GFP, and mCherry RNAi controls in all plates. This library is referred to as met-3.0 (Table S10). For both libraries, bacterial strains were arrayed in 96-well plates and stored as glycerol stocks.

C. elegans RNAi assays

Primary RNAi screens were performed as described previously (Conte et al., 2015; MacNeil et al., 2015). Briefly, confluent cultures of *E. coli* HT115 harboring the metabolic gene RNAi clones were seeded on to 96-well flat bottom plates containing NGM agar with 2 mM isopropyl β -D-thiogalactopyranoside (IPTG, US Biological, I8500) and 50 μ g/mL ampicillin (Sigma, A9518). Plates were kept overnight at room temperature and seeded with about 15 L1-arrested transgenic animals per well. Animals were allowed to develop for 48 h to reach the L4 stage, and visually screened for changes in intestinal GFP or mCherry fluorescence relative to vector control RNAi. The primary screen was performed three times. All RNAi clones causing at least one change in intestinal fluorescence with any promoter were retested in a matrix screen against all 19 transgenic animal strains in 35 mm plates as above, but with 30-40 animals per plate. RNAi clones causing a change in intestinal fluorescence in at least two of five experiments were considered hits (Table S2). Some plates or wells were not tested (NT) due to technical issues such as not having enough animals per well or poor growth of the *E. coli* RNAi clone. Each hit was given a score of 1 and the total score was divided by the total number of tests to indicate a confidence score of 0.4 (2 out of 5) to 1.0 (5 out of 5).

The transcription factor (TF) RNAi library was described previously (MacNeil et al., 2015). This library was screened three times as described above using 25–30 *Pacdh-1::GFP;spha-2(tm1420)* animals per well of a 24-well plate containing NGM agar with 2 mM IPTG, 50 μ g/mL ampicillin. The screen with *Pnhr-178::GFP* animals was performed with supplementation of 0.3 μ M antimycin A to the NGM agar. Any TF RNAi that caused a reduction of GFP expression in the presence of antimycin A in two out of two trials was called a hit.

Metabolic pathway enrichment analysis

The met-2.0 RNAi library contains 993 genes from iCEL1314 (Yilmaz et al., 2020), covering 85 metabolic pathways and categories (Walker et al., 2021). Of the 1,251 primary screen hits, 80.8% are in the iCEL1314 model (1011 hits, 383 unique genes), and function in 81 metabolic pathways and categories. For each pathway or category, the number of genes from iCEL1314 that were detected as interacting with each promoter out of total tested was determined. Hypergeometric distribution was used to determine statistically significant enrichment for each pathway or category.

Drug treatment

Stock solutions of 1M 2-thenoyltrifluoroacetone (TTFA) (Sigma, T27006) and 5 mM antimycin A (Sigma, A8674) were dissolved in dimethyl sulfoxide (DMSO) (Sigma, D4540). Stock solutions of 10 mM rotenone (Sigma, R8875) and 1 M sodium azide (Sigma, S2002), 1 M 3-nitropropionate (N5636-1G) were dissolved in sterile water. All stock solutions were stored at -20°C . Stock solutions were freshly diluted to the final concentration in NGM prior to plate pouring. All NGM/drug plates were made one day in advance of each experiment and stored at 4°C .

Bacterial growth assays with TTFA

E. coli HT115 containing vector plasmid was grown overnight in LB containing 50 μ M ampicillin at 37°C . The following day a dilution series was spotted in technical duplicate onto NGM plates with and without 2 mM IPTG and increasing doses of TTFA dissolved in 0.1% DMSO. Colonies were later counted by eye and normalized to the number of colonies on the untreated condition. To test bacterial growth with TTFA in liquid a 1/200 diluted bacterial subculture was treated with a titration of TTFA dissolved in 0.1% DMSO and optical density measurements were taken every 10 min by a Spark multimode microplate reader (Tecan) at 600 nm wavelength.

GFP quantification

The GFP fluorescence was quantified using a Tecan Infinite M1000Pro microplate reader as described (Bulcha et al., 2019). Briefly, five adult animals were put into wells with 35 μ L buffer (M9 buffer, 1 mM levamisole and 0.5% PEG) and GFP intensity was measured at 485nm/9nm excitation and 535nm/20nm emission. Each experiment was performed in biological triplicate with three technical triplicates each, and the

fluorescence intensity of each biological replicate was averaged. The average fluorescence intensity was used to plot fold change with respect to control.

qRT-PCR

qRT-PCR was performed as described previously (Bulcha et al., 2019). *cyc-1* RNAi was diluted 1:2 with vector RNAi to avoid developmental delays. Animals were washed in M9 buffer followed by RNA extraction using the Direct-zol RNA Miniprep Kit (Zymo Research, R2050), followed by DNase I treatment. cDNA was prepared from RNA using Oligo(dT) 12–18 Primer (Thermo Fisher, 18418) and M-MuLV Reverse Transcriptase (NEB, M0253S). qPCR was performed in biological triplicate with three technical replicates each per gene condition using the Applied Biosystems StepOnePlus Real-Time PCR system and Fast SYBR Green Master Mix (Thermo Fisher, 4385617). Relative transcript abundance was determined by using the $\Delta\Delta C_t$ method (Livak and Schmittgen, 2001) and normalized to averaged *ama-1* and *act-1* mRNA expression levels. Primer sequences are provided in Table S11.

Expression profiling by RNA-seq

RNA-seq was performed as described (Giese et al., 2020). Briefly, ~1,000 animals fed *E. coli* HT115 were harvested at the gravid adult stage. Animals were washed in M9 buffer followed by RNA extraction using the Direct-zol RNA Miniprep Kit (Zymo Research, R2050), followed by DNase I treatment. Multiplexed libraries were prepared using Cel-seq2 (Hashimshony et al., 2016). Three biological replicates were sequenced by BGI DNB-seq platform. On average ~6.5 million reads were obtained per sample. The libraries were demultiplexed and mapped as previously described (Giese et al., 2020). Differential gene expression analysis was performed by DEseq2 package R. Differentially expressed genes were selected based on a fold change ≥ 1.5 -fold or ≤ -1.5 -fold and P-adjusted value of < 0.05 . The RNA-sequencing data files were deposited in the NCBI Gene Expression Omnibus (GEO) under the following accession number: GEO Submission (GSE199433).

Antimycin toxicity assay

Eggs were collected using buffered bleach (5–6% sodium hypochlorite in 500 mM NaOH, freshly prepared), washed five times in M9 buffer, and allowed to hatch and synchronize to the L1 stage for 20 h in M9 buffer at room temperature. Approximately 100 synchronized L1 animals were added to *E. coli* HT115 RNAi vector control-seeded 48 well NGM agar plates containing various concentrations of antimycin A or DMSO as a vehicle control. After 48 h, animals that had developed past the L1 stage were counted. Each experiment was performed three independent times with eight technical replicates per experiment. Dose response curves were plotted with non-linear regression curve fitting as previously described (Watson et al., 2016).

Sequence alignment

Protein sequences were obtained from Wormbase version WB284 and aligned using the MUSCLE algorithm in MEGA11 (Edgar, 2004, Tamura et al., 2021).

QUANTIFICATION AND STATISTICAL ANALYSIS

The error bars represent the standard deviation from the average of three biological experiments. Data analysis & graph visualization was done with Prism 9 (GraphPad software). All fluorescent micrographs images were taken at the same exposure for each experiment. Images were taken at 10X magnification. Differentially expressed genes were selected based on a fold change 1.5-fold or more and P-adjusted value of < 0.05 . Differential gene expression analysis was performed by DEseq2 package R & the volcano plot was generated using VolcanoR. All statistical analyses are indicated in the legends to the relevant figure and in the corresponding STAR Methods section.